SQT

NASA CR-165160

(NASA-CR-165160) ANALYSIS AND DESIGN OF ION THRUSTERS FOR LARGE SPACE SYSTEMS Final Report, 23 May 1979 - 23 May 1980 (Xerox Electro-Optical Systems, Pasadena) 88 p HC A05/MF A01 CSCL 21C G3/20

N83-14159

Unclas 02300

# ANALYSIS AND DESIGN OF INERT GAS ION THRUSTERS

# FOR

# LARGE SPACE SYSTEMS

PREPARED FOR

LEWIS RESEARCH CENTER

NATIONAL AERONAUTICS AND SPACE ADMINISTRATION

CONTRACT NO. NAS3-21937

Final Report

November 1980

Edmund James

CONTENTS

CONTENTS (contd)

ILLUSTRATIONS

ILLUSTRATIONS (contd)

TABLES

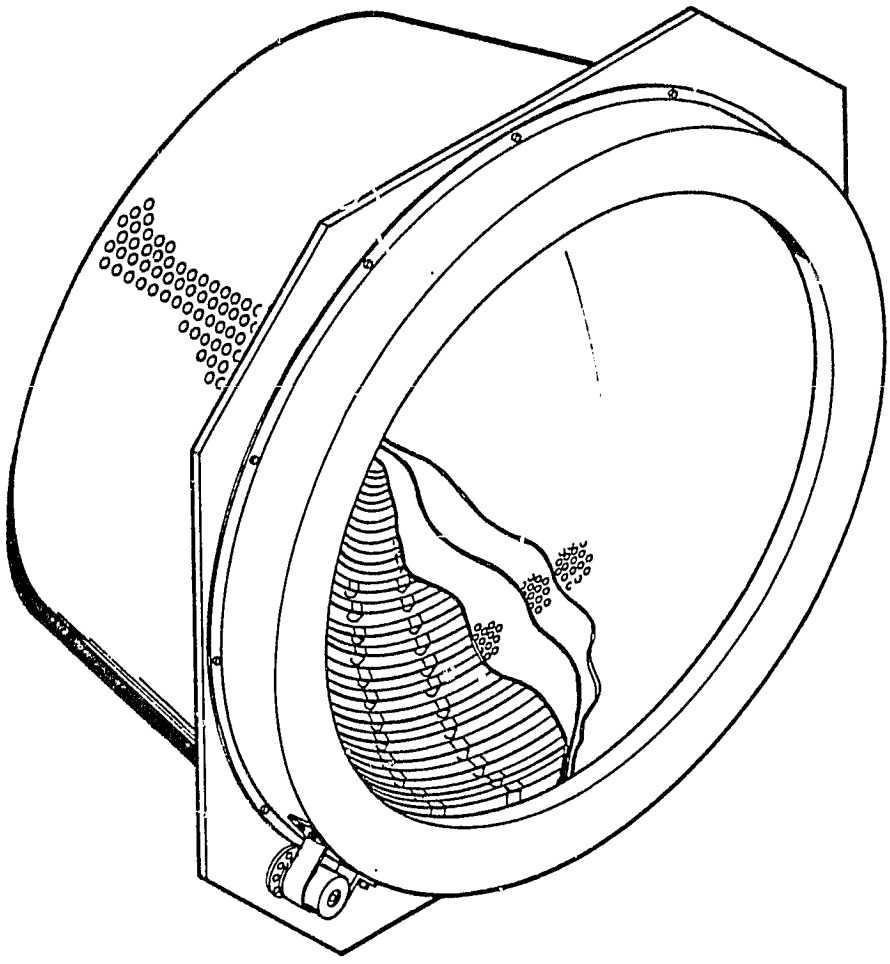

B 65874

50 cm Inert Gas Ion Thruster

# SECTION 1

## INTRODUCTION AND SUMMARY

Recent studies defining the requirements for Large Space Systems (LSS) have shown a sensitivity to propulsion system performance for both orbit transfer and stationkeeping functions. For the LSS, the NASA 30 cm mercury baseline may not result in optimum mission performance. For instance, the large quantities of propellant involved may dictate use of propellants other than mercury. An increase in power density may also be desirable.

In anticipation of these needs, a program was undertaken to analyze and define an efficient electrostatic ion thruster operating with inert gas propellants. The basic feasibility of such a thruster was established and a conceptual design of a 50 cm diameter ion thruster was developed. This thruster will operate at substantially higher thrust density than any previous electrostatic ion thruster. The thruster design selected was chosen for scaleability as well as performance. Once this thruster is developed, the basic principles involved will allow it to be scaled either up or down in size, and hence thrust, without requiring substantial additional development effort.

This effort began with an evaluation of various thruster concepts as described in Section 2. From this evaluation a concept was selected utilizing the magneto-electrostatic containment (MESC) variation of the periodic magnetic structure ion containment geometry. In the following phase of the program, trade studies and design calculations were performed for the various thruster components. Results are detailed in Section 3. A substantial effort was undertaken to analytically model the ion optics to ensure grid integrity at the high power densities involved. This analysis is summarized in Section 4.

The conceptual design of the 50 cm inert gas ion thruster is displayed in Section 5. For completeness, power processing requirements are given in Section 6.

# SECTION 2

# CONCEPT EVALUATION

The first step in developing the design of an inert gas thruster for use with large space structures was to select a plasma containment concept. In the concept evaluation phase, a literature survey was conducted; then containment techniques were evaluated and a concept selected for development into a thruster design.

## 2.1 LITERATURE SURVEY

The investigation into alternate plasma containment concepts included review of the electric propulsion literature, the Xerox and California Institute of Technology libraries, and computer search data from New England Research Applications Center (NERAC). Copies of promising literature identified through the study were then obtained. Several hundred abstracts were reviewed and many technical papers consequently selected for study. This effort did not identify any significantly new containment technique heretofore ignored by the electric propulsion community nor did it provide comprehensive new design data. Significant qualitative work was found, however.

Interesting publications identified included a substantial paper on plasma containment in cusp-shaped magnetic fields by Haines[6] of the Imperial College, London, and a collection of works by Leung,[12-15] who has been at UCLA and Madison and has worked with the Oak Ridge group. While at UCLA, Leung[15] did some experimental work demonstrating that the full line cusp was superior to the MacKenzie[16] point cusp for efficient plasma containment. This work provided the operational experience that supported our analytically based decision to

bypass the point cusp containment scheme in favor of the line cusp scheme, as discussed in the next section. The bibliography lists these and other contributing works.

## 2.2 CONTAINMENT TECHNIQUES

The literature review suggested that magnetic containment similar to that currently in use for electric propulsion held the most promise. The options available were an axial magnetic field structure as in the divergent field thruster or a periodic magnetic field structure as in the MESC thruster. The requirement for scaleability over a 4:1 size range and demonstrated superior ionization efficiency demanded selection of a periodic structure, with containment relying on the reflective properties of magnetic cusps.

Options available are listed in table 2-1 and shown in figure 2-1. The choice was between line cusp structure or a point cusp (checkerboard) structure like that proposed by K. R. MacKenzie.[16] The MacKenzie structure was intriguing, but was rejected after analysis of fabrication technique, probable response during launch vibration conditions, and experimental results from the literature.

TABLE 2-1

CONCEPTS FOR PERIODIC MAGNETIC STRUCTURE

Line Cusps
Magneto-Electrostatic Containment (MESC)
Multipole
External Magnets
Picket Fence
Point Cusps
Checkerboard

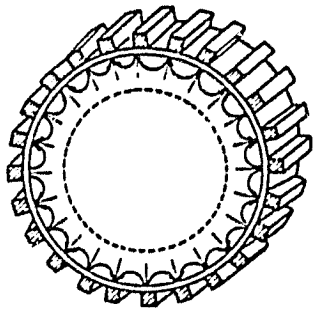

PICKET FENCE

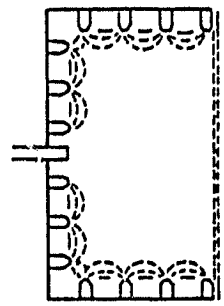

MULTIPOLE

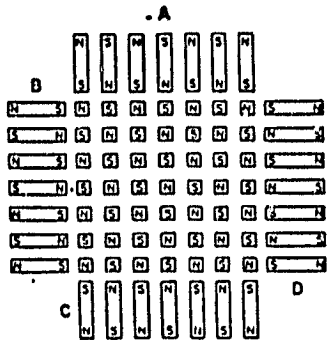


CHECKERBOARD

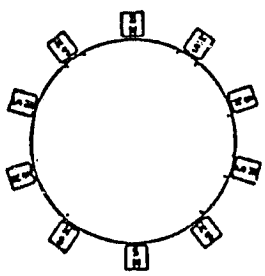

EXTERNAL MAGNETS

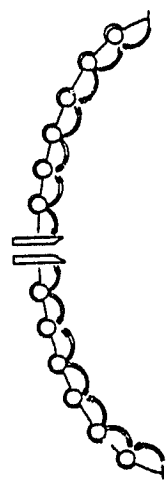

MESC

Figure 2-1. Ion Generation Techniques

Line cusps can be utilized either parallel with the thrust axis (picket fence) or perpendicular to it (MESC and Multipole). The parallel version had been operated in some laboratories but at the time of selection, not as a thruster. Analysis suggested that maintaining anode spacing on the rear wall would become difficult with this geometry. Two other factors were considered. With the parallel line cusp, control of the axial field would probably be difficult. The axial field is important in controlling electron flow from the cathode. The problem would be compounded should subsequent analysis indicate multiple cathodes were required. Also, operation with anodes positive with respect to the plasma is theorized to require a plasma viscosity effect to suppress contrarotating streams of plasma.[19] The axial or parallel line cusp geometry encourages plasma streaming perpendicular to the desired flow. The azimuthal, or perpendicular, line cusp geometry was thus selected for further consideration in developing a conceptual design.

Development work on periodic structure containment undertaken for NASA Lewis Research Center under Contract NAS3-21345 has indicated that ion containment is enhanced by strong magnetic fields. This result was used to narrow the selection further.

The external magnet concept was eliminated because of the difficulty of achieving high fields with this geometry unless a second shell was provided to reduce air gap losses and complete the magnetic circuit. With a second shell outboard of the magnets, the experimental flexibility of the external magnets was lost.

The final choice was between the multipole geometry with magnets parallel with the chamber walls and the MESC geometry with magnets perpendicular to the chamber walls. Figure 2-2, after Parker, illustrates the differences in flux density resulting from different geometries. While the demagnetizing geometry of an ion thruster reduces the effect shown in figure 2-1, the principle is still valid. In order to achieve the maximum flux density at the anodes, the MESC configuration was chosen for the conceptual design.

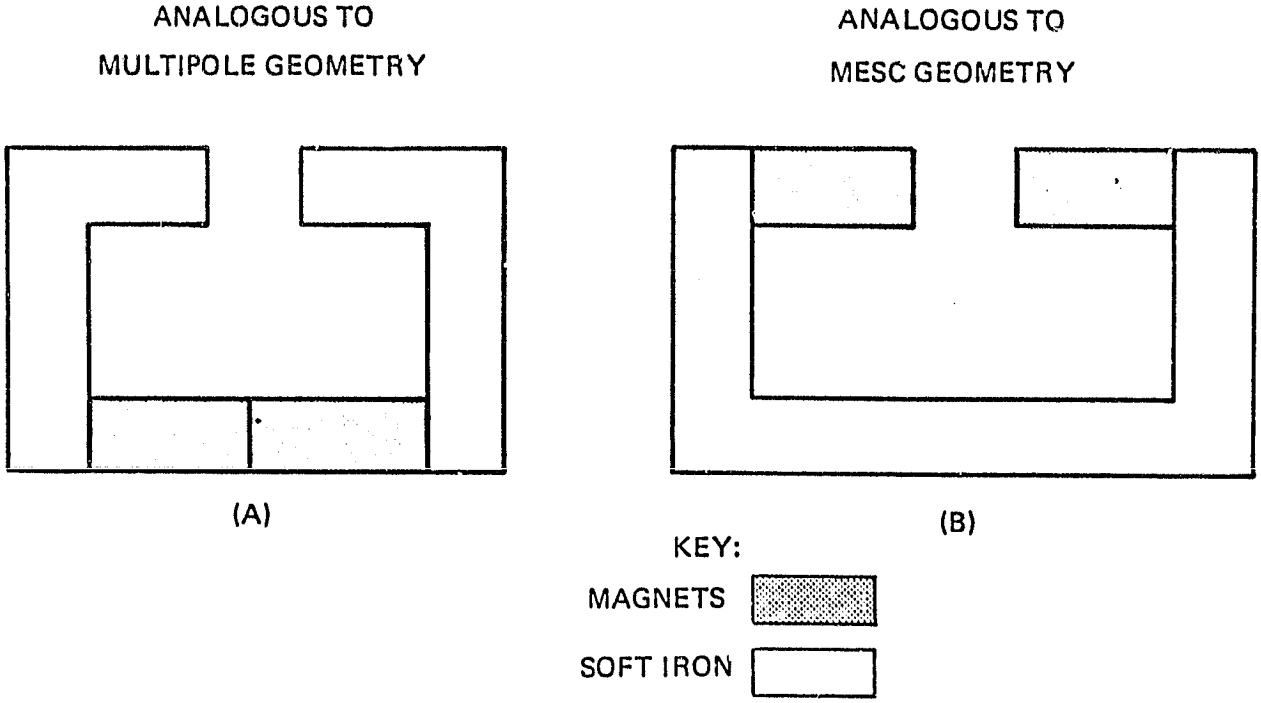


| | (A) | (B) |
|---|---|---|
| GAP DENSITY, GAUSS | 908 | 1,975 |
| POLE FACE DENSITY, GAUSS | 1,860 | 4,130 |
| MAXIMUM MAGNET DENSITY, GAUSS | 12,800 | 9,450 |
| RATIO OF TOTAL FLUX TO GAP FLUX | 14.1 | 4.78 |

After:

Parker and Studders, Permanent Magnets and Their Application, Wiley and Sons, NY 1962

Figure 2-2. Effect of Geometry on Flux Density

# SECTION 3

# ANALYSIS AND DESIGN

Selection of a containment scheme allowed development of the design concept to proceed. Analytical efforts were undertaken to support design decisions for thruster size, discharge chamber configuration, magnetic materials, cathode configuration, and anode configuration.

## 3.1 THRUSTER SIZE SELECTION

The guideline requirements specify thrust, specific impulse, and efficiency. These goals can be met with various choices of several parameters that affect thruster size. A program was developed to compute thruster diameter based on selection of optics apertures and center-to-center spacings, interelectrode spacing at operating temperature, discharge and keeper voltage, accelerator electrode voltage, and electrode thickness. From these parameters, a double ion factor was computed based on an unpublished model developed by Worlock and Ramsey under Contract NAS3-21345. Optics parameters were used to compute an effective electrode gap and hence perveance. Neutral efflux and mass efficiency were estimated based on experimental data with the 12 cm MESC thruster, figure 3-1. These were used to compute the screen potential, current density, and beam current. The computation is iterated to converge on a thruster diameter.

The flow diagram for this program is shown in figure 3-2. Results for several choices of center-to-center spacing and arc voltages are shown for argon in figure 3-3 and for xenon in figure 3-4. For argon operating at discharge potentials consistent with long life, the optimum thruster diameter is between 50 and 55 cm. For xenon, the

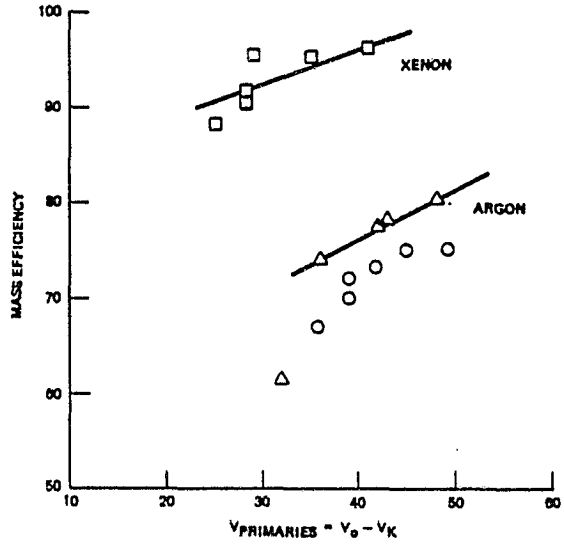


67518

Figure 3-1. 12 cm Mass Efficiency with Arc Voltage

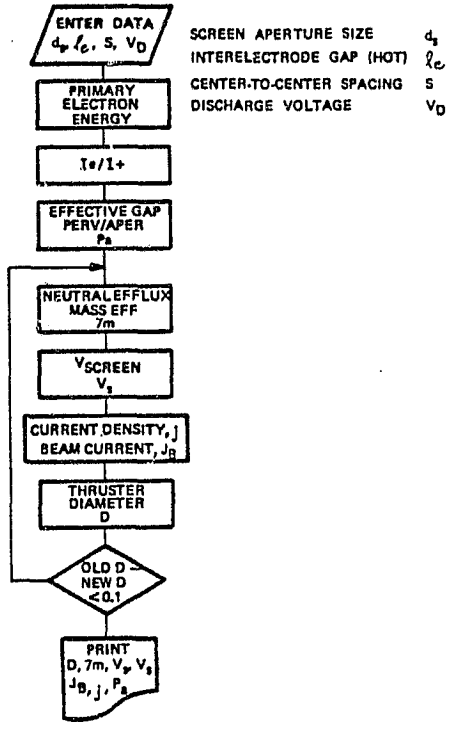


67515

Figure 3-2. Thruster Diameter Flow Diagram

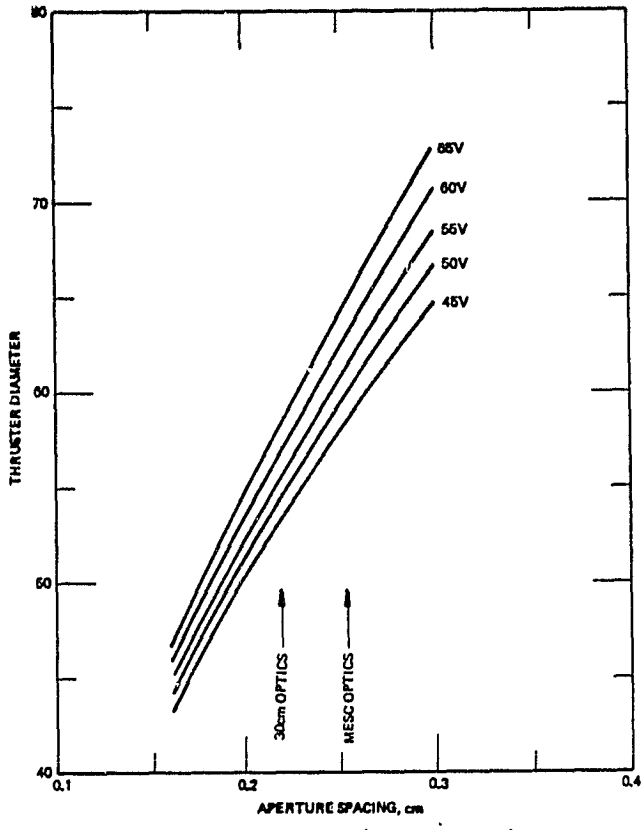


67519

Figure 3-3. Argon Thruster Diameter

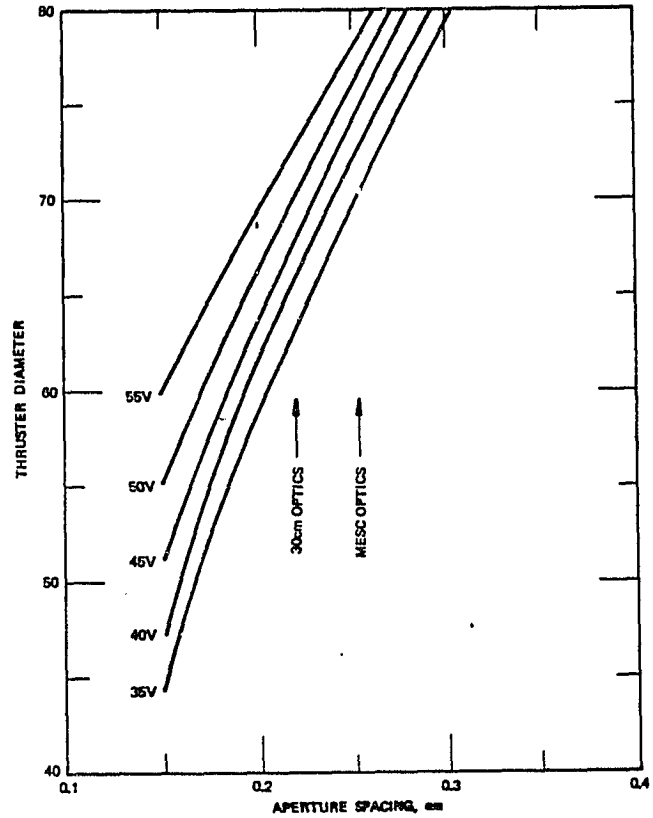


67520

Figure 3-4. Xenon Thruster Diameter

optimum is somewhat higher. In order to meet the additional contract requirement of using materials that are commercially available, 50 cm was selected as the thruster diameter for conceptual development.

## 3.2 DISCHARGE CHAMBER CONFIGURATION

Trade studies were conducted to identify a discharge chamber configuration that minimized cost and weight and maximized thruster performance. Discharge chamber optimization must be concerned with:

a. Minimizing ion recombination surface area
b. Minimizing structural weight
c. Permanent magnet shape mounting and support
d. Boundary anode mounting and support
e. Cathode mounting and support
f. Cathode flow distribution
g. Optics mounting and support
h. Anode feed supply mounting and support
i. Anode feed flow distribution
j. Discharge chamber heat rejection

An ion beam cross section was selected first. Figure 3-5 shows variations of the configuration looking into the thruster. All are compatible with the basic hexagon grid hole pattern with minor outside hole modifications for the circular and dodecagon cases. The polygon shapes are attractive from the point of view of magnet installation; however, minimum ion recombination area can be achieved with the circular cross section. This choice results in a slight reduction in magnetic field due to an imperfect magnetic circuit (using straight magnets on a curved surface). However, the large thruster diameter results in a very small air gap between magnet and chamber when magnet segments are limited to 2 to 3 cm. The resulting loss in magnetic field is acceptable.

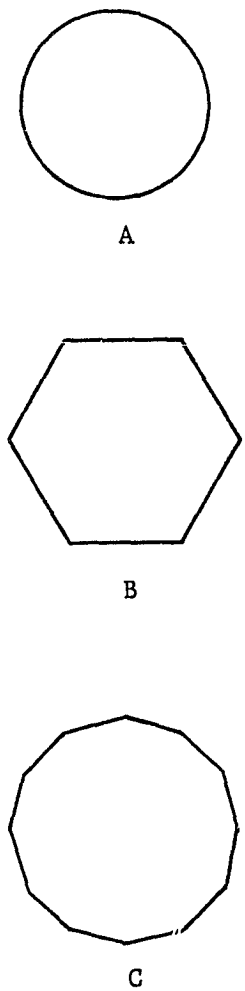


62640

Figure 3-5. Ion Beam Cross Sections

The discharge chamber axial cross section, which is the shape of the chamber at a section parallel to the thrust axis, was selected on the basis of maximizing the active area to loss area ratio. Here the active area is taken as the area available for ion extraction, the screen and open area, and the loss area is conservatively taken as the remaining surface area of chamber and screen grid. Table 3-1 shows results for candidate geometries. The dual cone is an approximation of the oblate spheroid that proved more difficult to fabricate; consequently, the oblate spheroid was selected.

TABLE 3-1

CANDIDATE DISCHARGE CHAMBER CONFIGURATIONS

| Chamber Axial Section | Depth (cm) | Active Area/ Loss Area | Normalized to Cylinder |
|---|---|---|---|
| Cylinder | 15 | 0.231 | 1.0 |
| Hemisphere | 25 | 0.250 | 1.08 |
| Oblate Spheroid | 15 | 0.317 | 1.37 |
| Dual Cone | 25 | 0.267 | 1.16 |
| Dual Cone | 15 | 0.341 | 1.48 |

To select a depth for the chamber, a computation of the mean free path to ionize was performed based on analysis by Masek.[18] Electron temperatures and distributions are not well known yet for argon and xenon in this configuration. The data spread available from MESC testing yields the results shown in table 3-2. Performance with chambers of 4.8 and 6 cm lengths suggested that a length comparable to the higher value of mean free path, or 2.5 times the lower value works well for xenon.

Argon, using the same criteria, should optimize between 15 and 20 cm depth. The thruster is intended as a laboratory instrument for operation with both argon and xenon. Since argon operation is expected to

dominate testing on cost grounds, a depth of 15 cm was selected as a practical compromise between competing requirements.

TABLE 3-2

MEAN FREE PATH TO IONIZE

| Specie | Discharge Potential (V) | Primary Energy (eV) | Mean Free Path to Ionize (cm) |
|---|---|---|---|
| Mercury | 36 | 30 | 5 |
| Argon | 53 | 30 | 6 to 20 |
| Xenon | 44 | 28 | 2 to 8 |

The selected discharge chamber configuration is summarized in table 3-3.

TABLE 3-3

SELECTED DISCHARGE CHAMBER CONFIGURATION

- o Laboratory Thruster
- o Compropromise Between Argon and Xenon Requirements
- o Diameter 50 cm
- o Length 15 cm
- o Configuration Oblate Spheroid

## 3.3 MAGNET MATERIAL SELECTION

Investigations conducted under NAS3-21345 strongly suggest that increased ion containment is achieved with higher magnetic fields and hence stronger magnets. Thus, the magnet material becomes an important thruster component. The magnetic geometry in a periodic magnetic structure containment scheme is highly demagnetizing; hence, a magnet material with high coersive force is required. Magnetic materials for use in ion thrusters must meet other

stringent requirements also. Among these are the ability to perform for 20,000 to 30,000 hours at temperatures up to 300°C with minimal loss in magnetic properties, survive launch vibration and shock requirements, and be chemically compatible with common propellants. For comparison, table 3-4 lists some of the more important properties of the candidate materials: platinum cobalt, samarium cobalt, and AlNiCo VIII. Figure 3-6 shows the B-H characteristics of these materials. Figure 3-7 indicates the relative weight and cost.

TABLE 3-4

PROPERTIES OF CANDIDATE MATERIALS

| Alloy | Energy Product | Residual Induction (Gauss) | Coersive Force (Oersteds) | Curie Temp. (°C) | Density (g/cc) |
|---|---|---|---|---|---|
| Platinum 77% Cobalt 23% | $9.5 \times 10^6$ | 6400 | 4300 | 480 | 15.4 |
| Samarium Cobalt | $18 \times 10^6$ | 8000 | 7000 | 750 | 8.2 |
| AlNiCo VIII | $5.5 \times 10^6$ | 7100 | 2000 | 845 | 7.3 |

From a weight and magnetic properties standpoint, samarium cobalt is the proper choice, and the cost, while not the lowest, is acceptable. Platcovar is second in magnetic properties but very expensive even without the volatile precious metals market. Experimental experiance with samarium cobalt indicated that material from some manufacturers did not match published thermal properties. An XEOS internal program examined various sources and identified a potential source for samarium cobalt. Short term thermal test results are given in figure 3-8. At this time, no long-term tests have been conducted; thus, AlNiCo was selected as the baseline magnetic material. However, it is hoped that continued testing will qualify samarium cobalt for thruster applications.

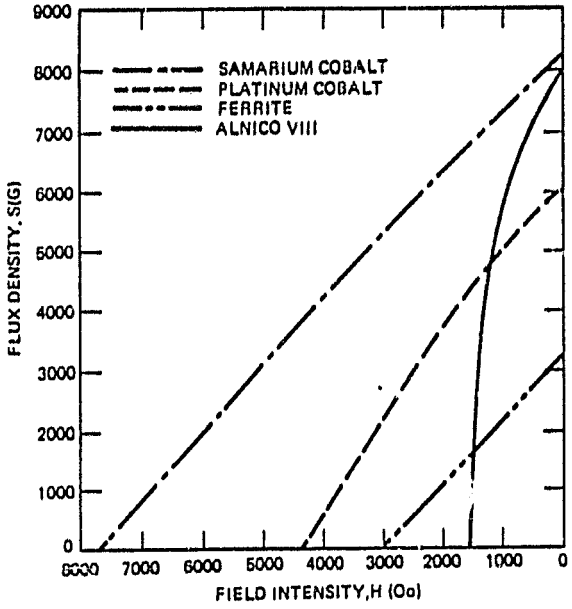


65878

Figure 3-6. B-H Diagram for Candidate Materials

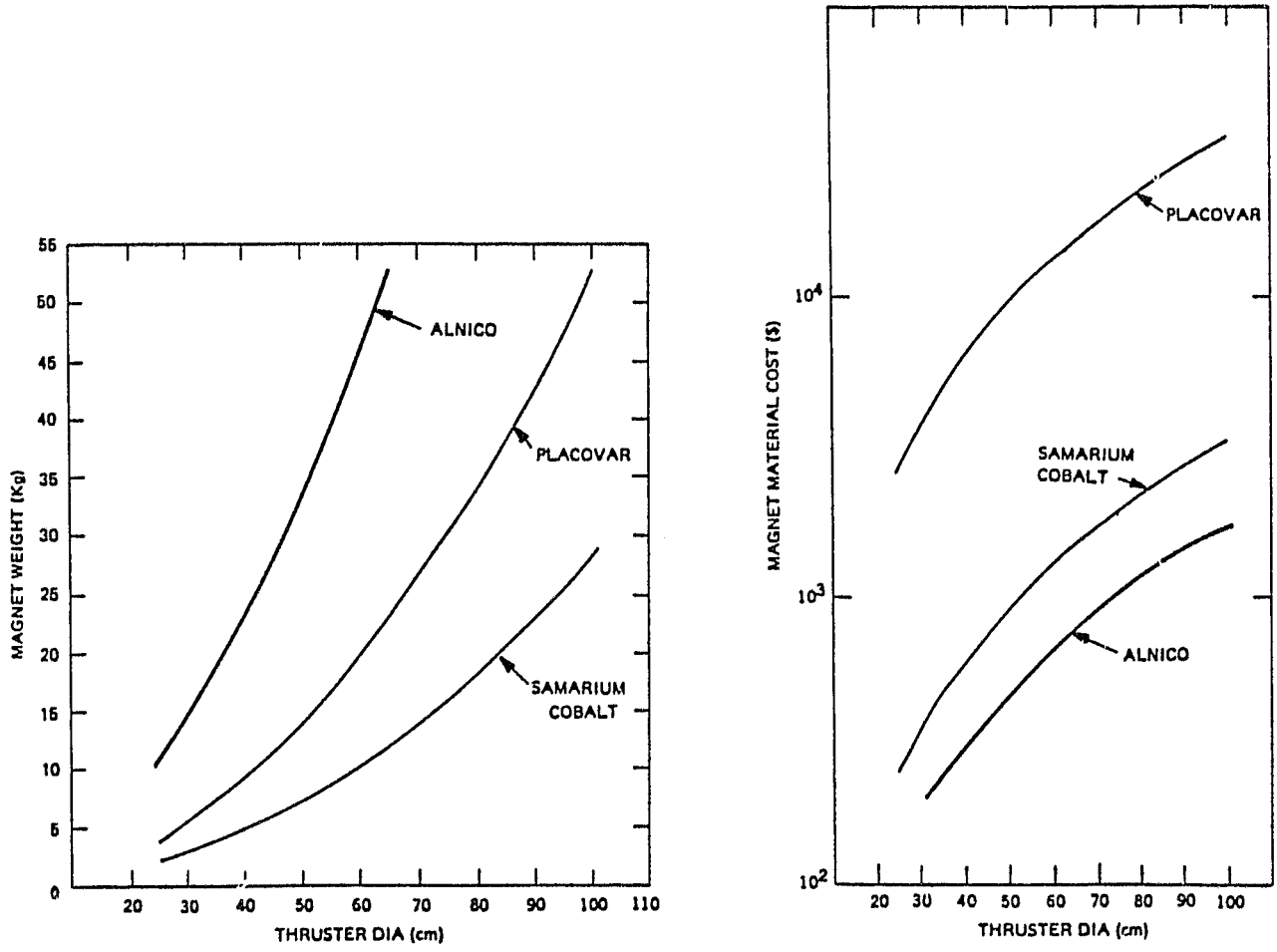


62635

Figure 3-7. Relative Weight and Cost of Candidate Materials

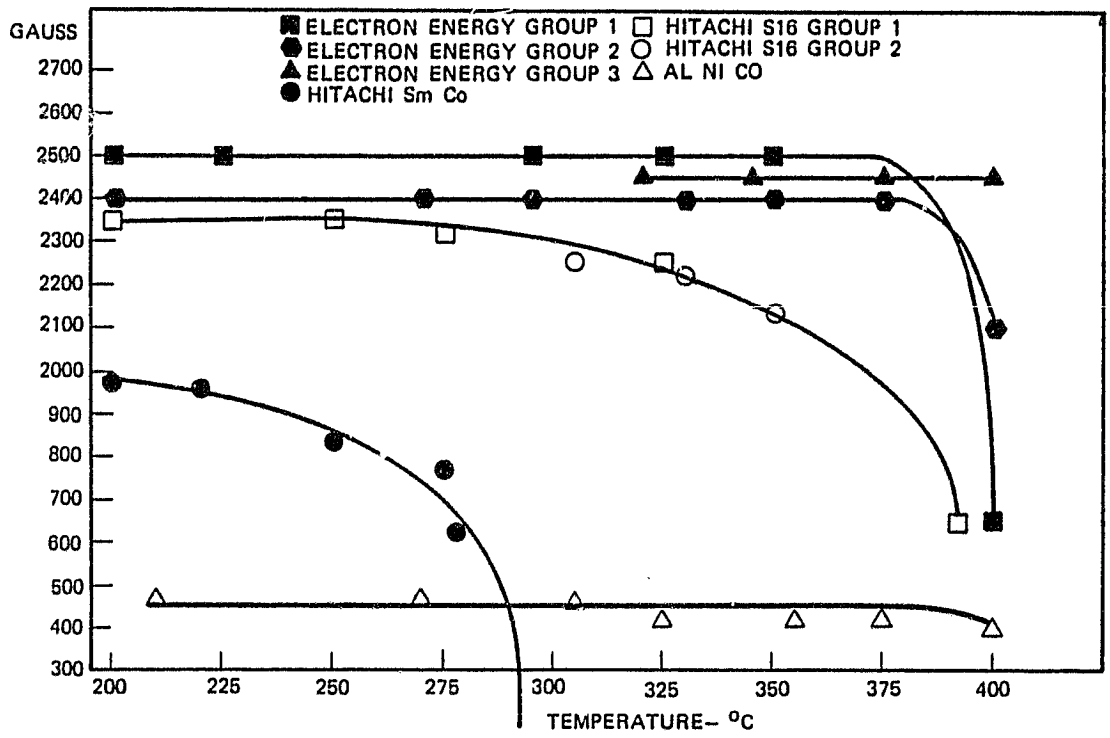


65912

Figure 3-8. Thermal Properties of Magnetic Materials

## 3.4 CATHODE/NEUTRALIZER CONFIGURATIONS

The cathode and neutralizer are similar in functional design and will be treated together. The principal difference between the two is the current capability required with the demand on the neutralizer much less than that on the main cathode. Also, the main cathode requires a baffle to separate the keeper plasma from the main discharge.

For a large thruster, scaling of the neutralizer is a matter of providing the appropriate electron flow. The main cathode must deliver enough electrons and must be able to deliver them to the full extent of the discharge chamber. This raises the question of a possible need for multiple cathodes. As is discussed in the following sections, a single cathode can be designed to provide satisfactory electron flow, and these will diffuse throughout the discharge chamber. Based on those results, the single versus multiple cathode was evaluated and the single cathode selected. The several considerations are shown in table 3-5.

### 3.4.1 CATHODE/NEUTRALIZER DESIGNS

Hollow cathode operation is being pursued by several workers in the field throughout the world. The literature indicates a general consensus regarding the emission mechanism involved as well as temperature and density gradients along the emitter surface for a given set of operating conditions. Typically, most of the electron emission originates from the downstream end of the emitter and is the result of field-enhanced thermionic operation. Emitter temperatures are maintained by ion bombardment from the dense plasma in the hollow cathode itself. Energy input from the plasma is balanced against emitter radiation and conduction losses and energy lost through the electron evaporation from the emitter surface. Electron energy is

TABLE 3-5

CATHODE TRADE TABLE

| Cathode Configuration | Positive Features | Negative Features |
|---|---|---|
| Single | 1. Easily controlled emission current | 1. Less reliable |
| | 2. Operate at design level emission | 2. Beyond existing ion thruster technology (size) (100A discharges in fusion research) |
| | 3. Symmetric field cancels and produced nonpeaked plasma distribution | 3. High thermal energy concentration in cathode region |
| | 4. Best performance | |
| Multiple | 1. Greater reliability | 1. Difficult to regulate emission and avoid cathode dominent mode |
| | 2. Distributed source of electrons in the discharge chamber | 2. Multiple cathode magnets produce a nonzero magnetic field in the bulk plasma region and a "peaked" distribution. Performance penalty. |
| | 3. Distribute cathode thermal load along the rear wall of the discharge chamber | 3. Slight increase in ionic wall recombination losses due to baffle housing surface area increase |
| | | 4. Needs more control circuitry and electrical isolation to control and balance emission |
| | | 5. Operates below design level emission |

delivered to the keeper and anodes outside the cathode structure while the radiation and conductive losses are reradiated and, to a lesser extent, conducted from the downstream end of the cathode. Most of the internal energy is radiated as hollow cathodes tend to be long (7.5 to 10 cm) thin wall (0.38 mm) tubes with small conductive paths.

Good emitter lifetime depends on maintaining the emitter surface at 1050°C or less. Operating temperatures in this realm have long projected lifetimes without excessive barium aluminate evaporation, according to the manufacturer's (Semicon) specification sheets. Using a Semicon emitter, Robinson[22] emperically derived a relationship between emission current and cathode life as a function of barium-aluminate usage. The emitter volumes for the main cathode and neutralizer were calculated from Robinson's model.

Neutralizer and cathode diameters were calculated from thermal consideration. Input energy to the emitter surface is a function of emission current. Siegfried,[23] Ferreria,[3] and Ramsey[24] empirically determined that the input energy to the emitter surface is directly proportional to the emission current. Assuming the thermal losses from the cathode are mostly radiative; the diameter should be directly proporational to the accepted emission operational level from the Stefan-Boltzmann relationship. Data for 0.32 cm argon cathode operation[25] and 0.64 cm argon cathode operation,[23] and 0.64 cm mercury cathode operation[28] were used to establish the ratio of cathode orifice plate-to-emission current needed to maintain emitter at 1000°C. The calculated ratios were used to determine the diameters of the cathode and neutralizer.

Orifice size was calculated from two considerations. First, the cathode structure thermal characteristics are similar to those of a classic blackbody where the orifice serves as the hole in the cavity walls and the orifice plate is one wall of the cavity. The larger the orifice

diameter the cooler the cathode operation for a given emission current. Secondly, the larger the orifice size the greater the mass flow needed to maintain the neutral density in the internal cathode plasma. However, larger cathode mass flow rates have a slightly negative impact on thruster performance from experimental data with different orifice diameters in a previous argon thruster program. In view of these tradeoffs, a large orifice was selected that would maintain plasma operating conditions within the cathode under the maximum anticipated emission current at minimum flows using the cathode pressure model developed by Ferreria.[2] This was found to agree with Dushman's[3] equation through orifices scaled to the 0.32 and 0.64 argon experimental data.

Cathode orifice plate thickness was selected on mechanical consideration. The orifice plate is uniformly heated by thermal radiation from the inside diameter of the emitter and internal plasma radiation. The orifice plate has a fairly uniform temperature across its surface with no regions of high thermal stress.

The thoriated tungsten orifice will be electron beam welded to the molybdenum tube. Material selection was based on temperature and erosion considerations observed in tests conducted in a parallel 12 cm inert gas ion thruster program. Tests conducted with tantalum and molybdenum cathodes found evidence of tantalum erosion by the barium aluminate emitter material under some operating conditions. Molybdenum tubing had no erosion under comparable operation and was selected for use in the advance thruster design.

Keeper electrode, baffle disk, and their mutual support tubes were designed to fit the anticipated operational temperature and energy levels in the cathode region. The keeper current should run between 4 to 5 amperes for the main discharge cathode and 0.8 to 1.2 amperes for the neutralizer. These current levels were calculated from experimental data based on constant electron current density at the orifice.

The baffle disk and baffle support nominally operate at cathode potential. The literature indicates this approach produced severe sputtering in several lifetime tests with mercury. This can be reduced by operating the baffle at keeper potential and reducing the potential difference between the discharge plasma and the structure. A companion 12 cm inert gas program ongoing at XEOS will conduct tests with an enclosed keeper and a keeper potential baffle in the future to evaluate the impact on performance. If no negative impact is seen, the keeper potential baffle will be incorporated into the 50 cm thruster design.

The resulting designs for the cathode and neutralizer are shown in figures 3-9 and 3-10. Design details are listed in tables 3-6 and 3-7.

### 3.4.2 ELECTRON DIFFUSION

In order to determine the ability of a central cathode to deliver electrons to the outer areas of the discharge chamber, the diffusion of electrons in an inert gas plasma was examined. Electron diffusion across the magnetic field at the boundary of a periodic magnetic containment scheme, such as the MESC or the Multipole, has been treated in considerable detail elsewhere and the containment of primary energy electrons is well established. The transport of electrons through bulk plasma has also been examined by many authors including classical treatments by Spitzer[33] and electric propulsion oriented work by Kaufman. For this analysis, we selected work of Brown[1] since it is based on experimental data for both argon and xenon.

Mapping the magnetic field within the 12 cm MESC thruster indicates most of the volume away from the boundary and cathode pole piece exhibits very low axial magnetic field components, less than a millitesla. Thus, the field free diffusion equation should provide a reasonable approximation.

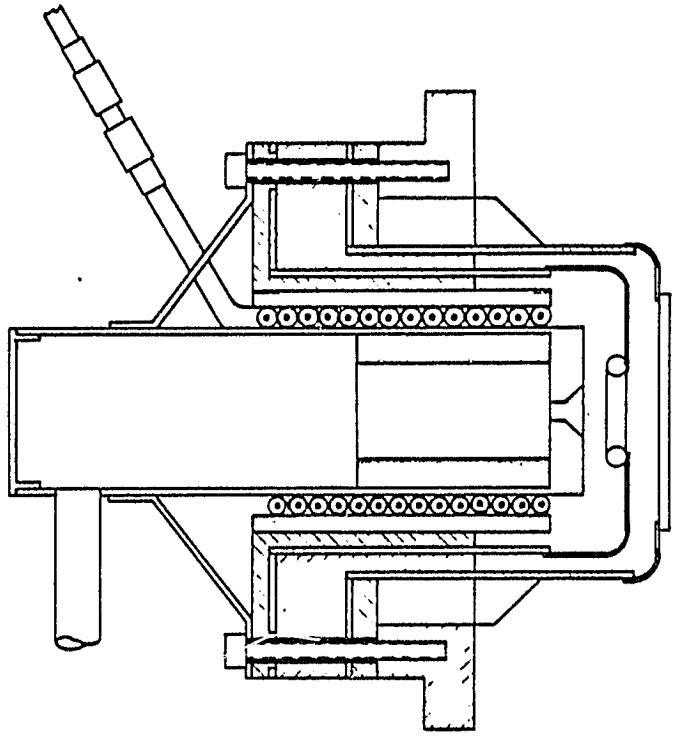

65882

Figure 3-9. Cathode Detail, 50 cm Thruster

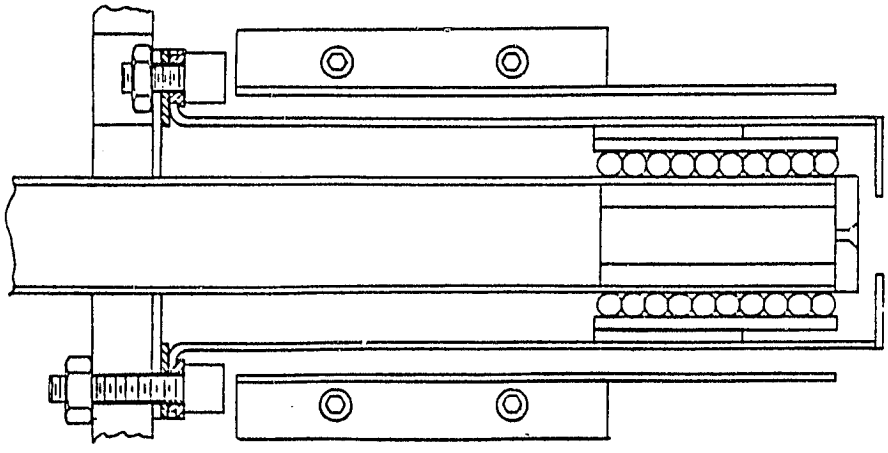


65917

Figure 3-10. 50 cm Thruster Conceptual Design

TABLE 3-6

CATHODE DIMENSIONS

| Function | Neutralizer | Cathode |
|---|---|---|
| Orifice Plate Diameter (cm) | 1.3 | 2.2 |
| Orifice Diameter (mm) | 1.0 | 2.2 |
| Emitter O.D. (cm) | 1.1 | 2.1 |
| Emitter I.D. (mm) | 6.4 | 16.5 |
| Emitter Length (cm) | 2.5 | 3.8 |
| Baffle Tube Diameter (cm) | N/A | 4.5 |
| Baffle Disk Diameter (cm) | N/A | 3.2 |
| Keeper Ring Diameter (cm) | 1.1 | 2.1 |
| Keeper Tube Diameter (cm) | 2.5 | 3.8 |

TABLE 3-7

CATHODE ASSEMBLY CONCEPTUAL DESIGN

| Component | Selection |
|---|---|
| Cathode Diameter | 2.2 cm |
| Cathode End Plate | Thoriated tungsten |
| Cathode Orifice | 2.2 mm with 2.5 cm countersink |
| Cathode Tube | 2.2 cm diameter |
| Heater | Coaxial tantalum clad tungsten-rhenium, 2.7 mm diameter with 0.76 mm center conductor |
| Keeper | Tantalum wire 2.5 mm diameter formed in a ring 1.5 cm outside diameter, 0.95 cm inside diameter |
| Baffle Disk | Tantalum, 3.2 cm diameter, 1.5 mm thick |
| Emitter | Impregnated tungsten |

In an ionized gas the flow of electrons, $\Gamma$, is described by the sum of a diffusion and a mobility term, so that

$$\vec{\Gamma} = -D\vec{\nabla}n_e - \mu n_e \vec{\nabla}V$$

where

$D$ = diffusion constant
$n_e$ = electron density
$\mu$ = mobility constant
$V$ = applied field

Looking at the case within the plasma, the field is essentially zero, so for one dimension in cylindrical geometry

$$\Gamma = -D \frac{dn_e}{dr}$$

Brown notes that, where electrons and ions are in thermal equilibrium, the diffusion is ambipolar and

$$D_a \approx v^2/3\nu_m$$

(It may be noted that this has the form of Kaufman's classical diffusion constant, $D = 2kT/3m\nu$.)

Brown further notes that

$$v^2/3\nu_m \approx \frac{v}{3 p_o p_m}$$

so

$$D_a \approx \frac{v}{3p_o P_m}$$

where

$D_a$ = ambipolar diffusion constant
$v$ = electron velocity
$\nu_m$ = collision frequency for momentum transfer
$P_o$ = pressure
$P_m$ = probability of a momentum transfer collision

Using data in Brown for $P_m$ and a pressure of $5 \times 10^{-5}$ torr, the diffusion constants are:

For a 40 V argon discharge $D_a \approx 2 \times 10^9$ cm$^2$/s
For a 30 V xenon discharge $D_a \approx 1 \times 10^9$ cm$^2$/s

From Langmiur probe data collected by Ramsey[24] for the MESC thruster

$$\frac{\Delta n_e}{\Delta r} \approx \frac{1 \times 10^{10} \text{ electrons/cm}^3}{5 \text{ cm}} = 2 \times 10^9 \text{ electrons/cm}^4$$

so that

$$\approx 4 \times 10^{18} \text{ electrons/cm}^2\text{/s}$$

or

$$\approx 0.6 \text{ A/cm}^2$$

For the 50 cm thruster, the area of the discharge, excluding the screen, is approximately 300 cm$^2$, so the arc should be able to conduct 2000A or 20 times the required current.

### 3.4.3 PROPELLANT DIFFUSION

Having adequate primary electrons throughout the plasma is useful only if there are neutral atoms to ionize. Following Dushman, the mean free path of an average argon neutral is 50 cm. Since the discharge chamber depth is 15 cm, most neutrals will traverse the chamber

without a collision. The optimum configuration for propellant entry remains to be determined experimentally, however, the most promising approach appears to be dual feed rings, one relatively near the cathode with flow directed downstream and one at the outer circumference of the discharge chamber. The outer ring will have a slight back feed to direct neutrals across the discharge chamber, increasing the probability of ionization.

## 3.5 ANODE CONFIGURATION

The anode design must meet several requirements. The critical edge, the edge that cuts the critical magnetic field line in the containment geometry, must be well defined and easily adjusted. The total anode cross section must be able to carry its share of discharge current. Finally, the anode height must be adjustable for thruster optimization.

Several anode designs were evaluated. These are listed in table 3-8. For this design, which is intended as a developmental thruster, the flat anode design was selected as the most versatile. The more complicated geometries offer more rigidity as well as slight improvements in performance, and may subsequently prove appropriate for flight hardware.

The anode insulators are designed for ease of adjustment of the anode height. Each insulator is shadow shielded to protect against buildup of thin conductive film. Two types are required, one for the basic anode array and one for support of the anode potential propellant delivery system, or main feed. Figure 3-11 shows details of these two insulating assemblies.

TABLE 3-8

ANODE DESIGN TRADEOFFS

| Anode Type | Positive Features | Negative Features |
|---|---|---|
| "U" or "⊥" Section Anode | 1. Perpendicular to the magnetic field. Improves sensitivity to adjustment.<br>2. Reasonable performance can be achieved with weak boundary magnetic fields. | 1. Difficult to fabricate.<br>2. Difficult to adjust. |
| Flat or Half Round | 1. Easy to fabricate.<br>2. Easy to adjust.<br>3. Produces good performance in strong magnetic field. | 1. Less sensitivity in anode placement.<br>2. Reduced performance in weak boundary magnetic field. |

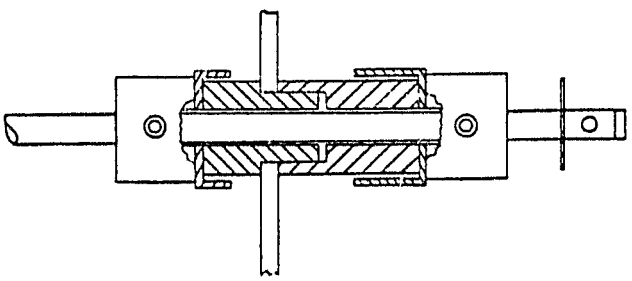


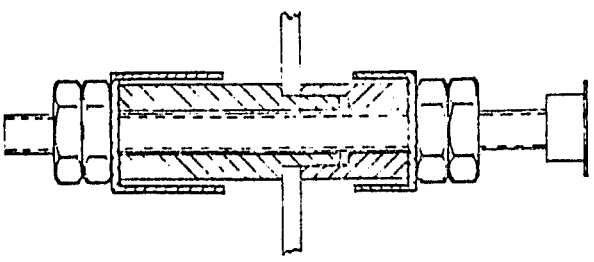


65916

Figure 3-11. 50 cm. Thruster Anode Details

# SECTION 4

# SUPPORTING ANALYSIS

This section documents the thermal and structural analysis performed for the initial design work on a 50 cm ion thruster. The power dissipation from the engine is estimated to be 4500W at full power. The analysis revealed that engine surface area is inadequate to radiate this energy at acceptable thruster temperatures. It is thus necessary to enhance the heat removal from the thruster. An active cooling loop was selected as the most feasible approach because the technology is available. A liquid coolant will be pumped through coils attached to the outer surface of the discharge chamber then to a remote space radiator.

The majority of the analysis time was spent on the ion optics assembly to find a workable design. To force uniform distribution of heat and stress in the grids, 48 bolts are used around the circumference (approximately every 3.5 cm). The requirement is to produce a design with acceptable stress levels without contact of the grids induced by thermal expansion which simultaneously maintains proper optical alignment. In the analysis, a uniform spacing of 0.1 cm was used between the three grids. The same spacing was used in the grid thruster analysis.

A primary requirement on the active cooling system will be to minimize thermal gradients both axially and circumferentially to hold the boundary conditions for which a successful analytical design was achieved.

During the initial part of the study, the optics assembly was assumed rigidly bolted to the discharge chamber. It was learned during the analysis that the fixed boundary caused unacceptably high stresses in the grids, so a slip joint was incorporated.

## 4.1 OPTICS THERMAL ANALYSIS

### 4.1.1 ANALYTICAL APPROACH

The Control Data Corporation (CDC) Mitas II Thermal Analysis Program was used to compute the temperatures for the ion optics assembly. The temperature analysis was then used as input for the structural analysis discussed in Section 3.0.

The Mitas II Program is a general software code designed to solve lumped-parameter, i.e., resistor-capacitor, network representations of thermal systems. The model network for the ion optics assembly is shown in engineering units in figure 4-1. The model consists of 33 diffusion anodes and three arithmetic (fixed temperature) anodes.

The principal assumptions in the analysis are summarized below:

a. Thermal symmetry was assumed at each bolt hole, thus a 1/48 pie-shaped section was used in the analysis. Uniform contact was assumed to be generated circumferentially by the bolts, thus thermal gradients exist only radially and axially.

b. Thermal conductivity of molybdenum was input as a function of temperature (Array 1). Constant values were used for the other materials because of their smaller temperature range. Scaling factors were used to account for the grid transparency.

c. The discharge chamber was held at a constant temperature to within 1.3 cm of the grid mount location. This assumes the active cooling loop carries the heat away to a space radiator and minimizes the circumferential thermal gradients.

SECURITY CLASSIFICATION

CHAMBER ℄

Figure 4-1

THERMAL IONIZ. CINEMATIC

PERFORATION PATTERN 1

GENERAL NOTES:
DIMENSIONS IN INCHES
DIFFUSION NODES ● 1-33
ARITHMETIC NODES (VV) (EA) (I)



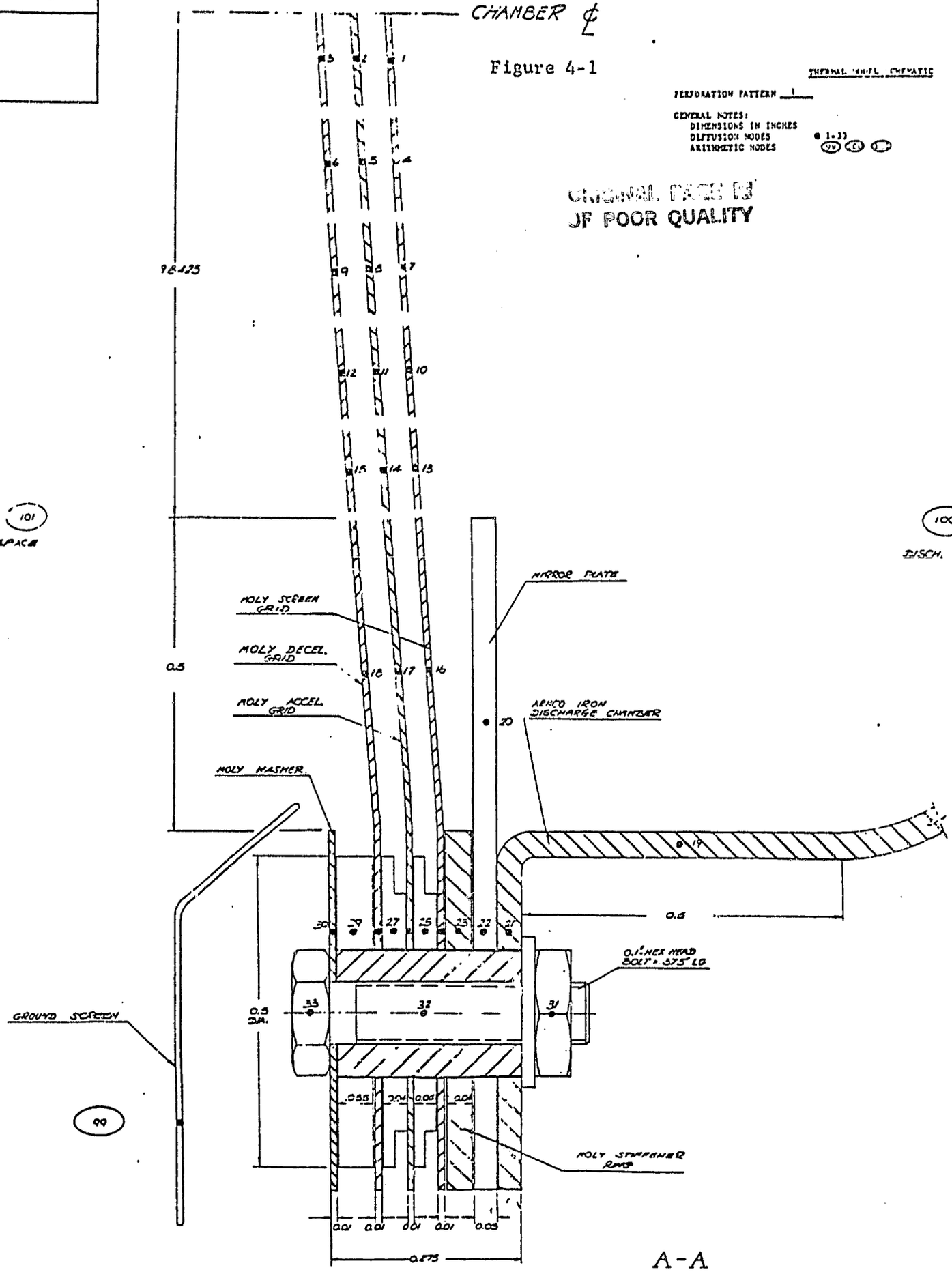


A-A
SCALE 10:1

d. The discharge chamber is a complex radiation source, not easily modelled. For an approximation, the inner surface was assumed to be at a single, constant temperature, and the surface emissivity was taken as 0.30.

e. The ground screen was held fixed at 38°C, with an emissivity of 0.85 (anodized aluminum).

f. Molybdenum emissivity was taken as 0.15.

g. The emissivity of the electrodeless nickel coating the Armco iron was taken as 0.15.

h. The grid transparencies used were:

- Screen 69 percent
- Accelerator 19 percent
- Decelerator 69 percent

i. An interface conductance of 0.57 $W/cm^2$ °C was assumed at all contact surfaces in the attachment area. This is a conservatively low value because of the high compression stress generated by the bolts. For the thermal analysis where the optics assembly is free to move due to thermal expansion, the relative motion is between the screen grid and mirror plate. No contact was assumed between these two surfaces; i.e., the only heat transfer mechanism is by radiation.

For the two grid cases that were analyzed, the same model was used, except that the nodes (3, 6, 9, 12, 15, 18), which represent the decelerator grid, were removed. The radiation analysis of the remaining grids was corrected appropriately.

Toulokian,[34] "Thermophysical Properties of Matter," was used as the source for thermodynamic properties. Analysis was carried out only at the full power condition.

### 4.1.2 DISCUSSION OF RESULTS

The basic model design is shown in figure 4-1. Table 4-1 presents a matrix of the various configurations analyzed. This table is oriented toward the structural analysis of Section 3, but also serves as a key

TABLE 4-1

ADIT STRUCTURAL CONFIGURATIONS ANALYZED

| CASE NO. | NO. OF GRIDS | DISCHARGE CHAMBER TEMP (C) | GRID THICKNESS (MM) | RADIUS OF CURVATURE (CM) | DISH DEPTH (CM) | THERMAL FIGURE NO. | PERFERATION PATTERN | OPTICS ASSEMBLY BOUNDARY CONDITION | COMMENTS |
|---|---|---|---|---|---|---|---|---|---|
| 0 | 2 | 170 | .38 SCREEN .25 ACCEL | 55 | 2.1 | 3 | | | 30 CM TEST CASE REFERENCE |
| 1 | 3 | 200 | .25 | 65 | 5.0 | 4 | 1 | FIXED | |
| 2 | 3 | | .25 | 55 | | | 1 | FIXED | NOT ANALYZED |
| 3 | 3 | | .25 | 48 | | | 1 | FIXED | NOT ANALYZED |
| 4 | 3 | 250 | .25 | 65 | 5.0 | 5 | 1 | FIXED | |
| 5 | 3 | 300 | .25 | 65 | 5.0 | 6 | 1 | FIXED | |
| 6 | 3 | 350 | .25 | 65 | 5.0 | 7 | 1 | FIXED | THERMAL ANALYSIS ONLY |
| 7 | 3 | 200 | .38 | 65 | 5.0 | 8 | 1 | FIXED | |
| 8 | 3 | 200 | .51 | 65 | 5.0 | 9 | 1 | FIXED | |
| 9 | 2 | 200 | .25 | 65 | 5.0 | 10 | 1 | FIXED | |
| 10 | 2 | 200 | .38 | 65 | 5.0 | 11 | 1 | FIXED | THERMAL ANALYSIS ONLY |
| 10a | 2 | 200 | .51 | 65 | 5.0 | 12 | 1 | FIXED | THERMAL ANALYSIS ONLY |
| 11 | 2 | 200 | .38 SCREEN .25 ACCEL | 65 | 5.0 | 13 | 1 | FIXED | THERMAL ANALYSIS ONLY |
| 11a | 2 | 200 | .38 | 95 | 3.35 | 11 | 1 | FIXED | EFFECT OF RADIUS CHANGE ON TEMPERATURE DEEMED NEGLIGIBLE |
| 11b | 2 | 200 | .51 | 95 | 3.35 | 12 | 1 | FIXED | EFFECT OF RADIUS CHANGE ON TEMPERATURE DEEMED NEGLIGIBLE |
| 12 | 3 | 200 | .38 | 65 | 5.0 | 8 | 1 | FREE | BOUNDARY FIXED IN THERMAL ANALYSIS |
| 13 | 3 | 200 | .25 | 65 | 5.0 | 14 | 2 | FREE | BOUNDARY FIXED IN THERMAL ANALYSIS |
| 14 | 3 | 200 | .25 | 65 | 5.0 | 14 | 2 | FIXED | |
| 15a | 3 | 200 | .38 | 95 | 3.35 | 15 | 2 | FREE | a) SAME COMMENT AS FOR CASE 11a<br>b) BOUNDARY FIXED IN THERMAL ANALYSIS |
| 15b | 3 | 200 | .38 | 95 | 3.35 | 15 | 2 | FIXED | SAME COMMENT AS FOR CASE 11a |
| 16 | 3 | 200 | .38 | 105 | 3.0 | 15 | 2 | FIXED | SAME COMMENT AS FOR CASE 11a |
| 17 | 3 | 200 | .25 | 65 | 5.0 | 16 | 2 | FREE | THERMAL ANALYSIS ONLY |

NOTE: UNLESS OTHERWISE STATED, THERMAL CONFIGURATION IS THE SAME AS THE STRUCTURAL CONFIGURATION.

to the thermal analysis shown in figures 4-2 through 4-15. To obtain some insight into the validity of the thermal modeling of the grid system, experimental temperature data were taken for the LeRC 30 cm thruster grid system at full power and correlated with analysis. The thermal model illustrated in figure 4-1 was modified as follows to simulate the 30 cm thruster:

- Grid diameter reduced from 50 cm to 30 cm
- Grid thickness corrected
- Decelerator grid removed

No attempt was made to simulate the very complex grid support structure of the 30 cm thruster. The results of this analysis are shown in figure 4-2. Excellence correlation with the experimental results were obtained in the area of interest away from the grid attachment. The thermal analysis of the 50 cm thruster is shown in figures 4-3 through 4-15. The figures are designed to be self-explanatory. Configuration variables were discharge chamber temperature, grid thickness, number of grids (2 or 3), grid radius of curvature, perforation configuration (two cases), and fixed or free floating attachment of the optics assembly to the discharge chamber. The model treats the case where apertures are aligned along radii of grid curvature. Compensation for beam diverence was not treated at this level of modeling since only second order effects on transmissivity and conductance would result. Radii of curvature between 65 and 105 cm were studied. A diameter toward the larger side of this range will most likely be used because of manufacturing considerations. A calculation of the input thermal parameters for the larger radii indicated small changes; thus the effect on temperature was deemed well within the accuracy of the analysis and a radius of 65 cm was used throughout the thermal analysis. However, the structural model was corrected for radius changes. The two grid perforation patterns which were analyzed may be understood by comparing figure 4-1 with figure 4-13.

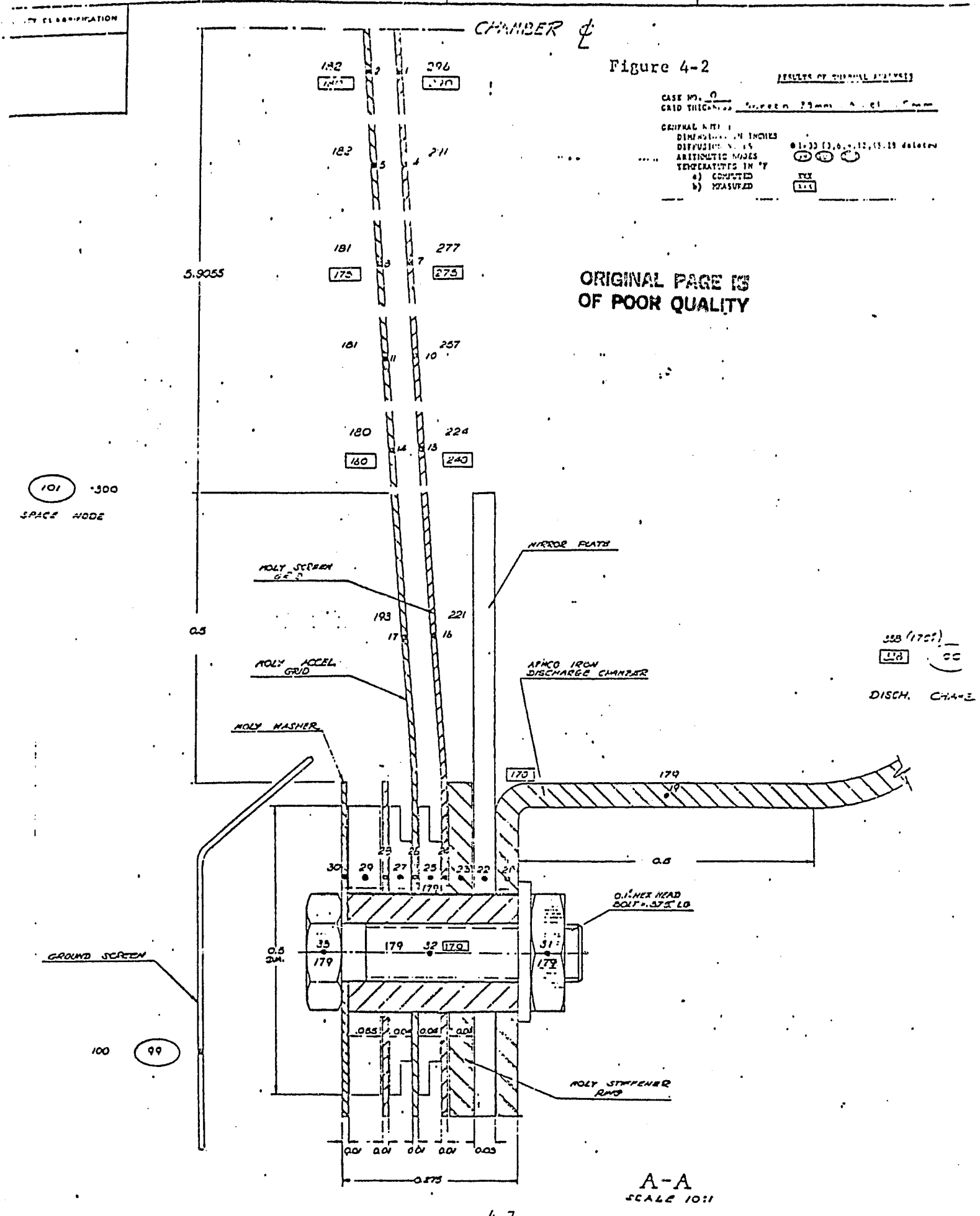


Figure 4-2

RESULTS OF THERMAL ANALYSIS

CASE NO. 0
GRID THICKNESS .040 in .79mm .061 1.5mm
ORIGINAL UNITS
DIMENSIONS IN INCHES
DIFFUSION NODES @1.33 (3,6,9,12,(15,18 deleted
ARITHMETIC NODES (2) (5) (7)
TEMPERATURES IN °F
a) COMPUTED XXX
b) MEASURED [XXX]

ORIGINAL PAGE IS
OF POOR QUALITY

SECURITY CLASSIFICATION

Figure 4-3

RESULTS OF THERMAL ANALYSIS

CASE NO. 1
PERFORATION PATTERN 1
GRID THICKNESS .26 mm
BOUNDARY CONDITION Fixed

GENERAL NOTES:
DIMENSIONS IN INCHES
DIFFUSION NODES ●1-33
ARITHMETIC NODES (1) (2) (3)
TEMPERATURES IN °F, XXX

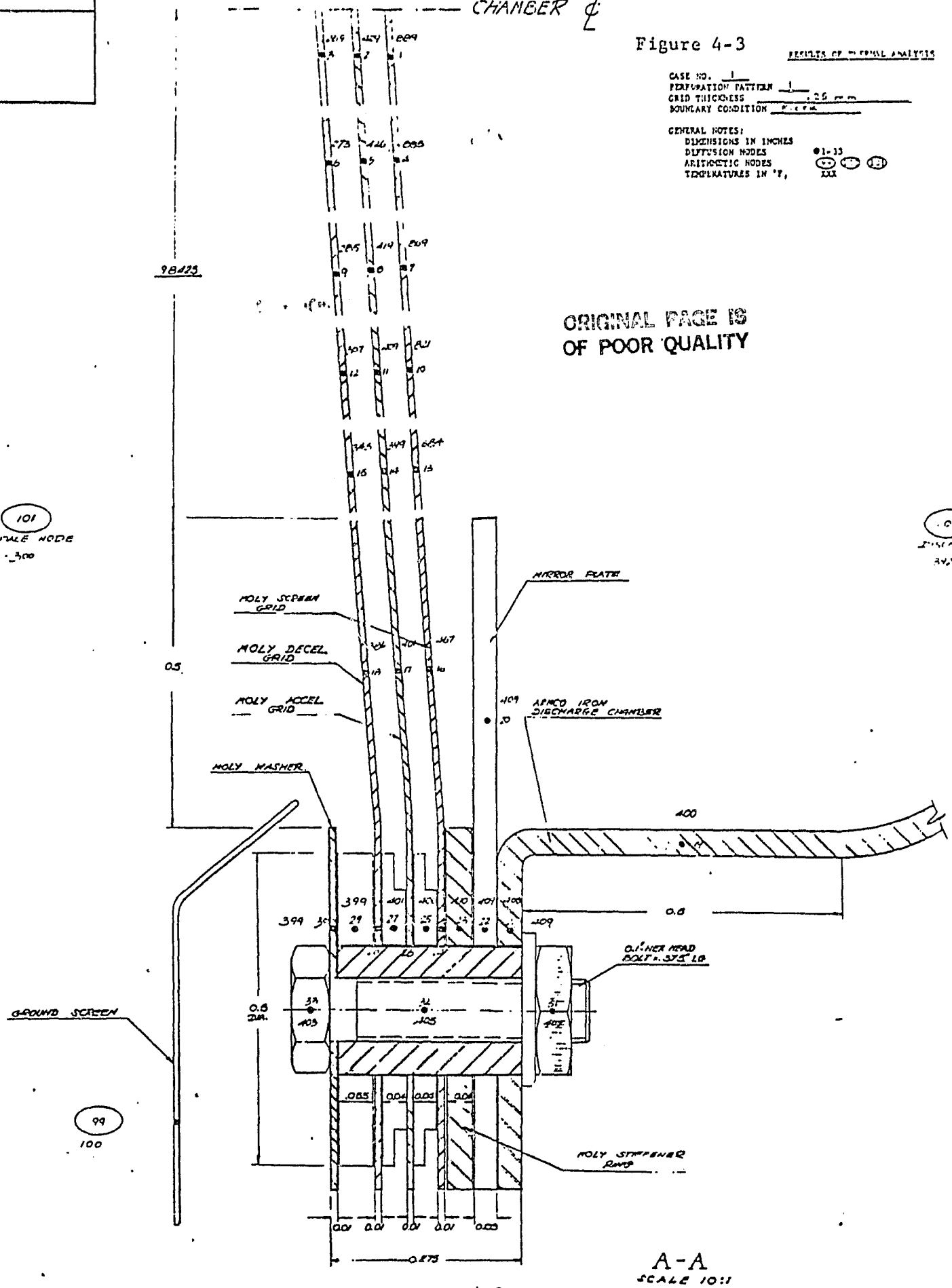

CHAMBER ℄

Figure 4-4

RESULTS OF THERMAL ANALYSIS

CASE NO. 4
PERFORATION PATTERN 1
GRID THICKNESS .25 mm
BOUNDARY CONDITION Fixed

GENERAL NOTES:
DIMENSIONS IN INCHES
DIFFUSION NODES ●1-33
ARITHMETIC NODES (40) (10) (11)
TEMPERATURES IN °F, XXX



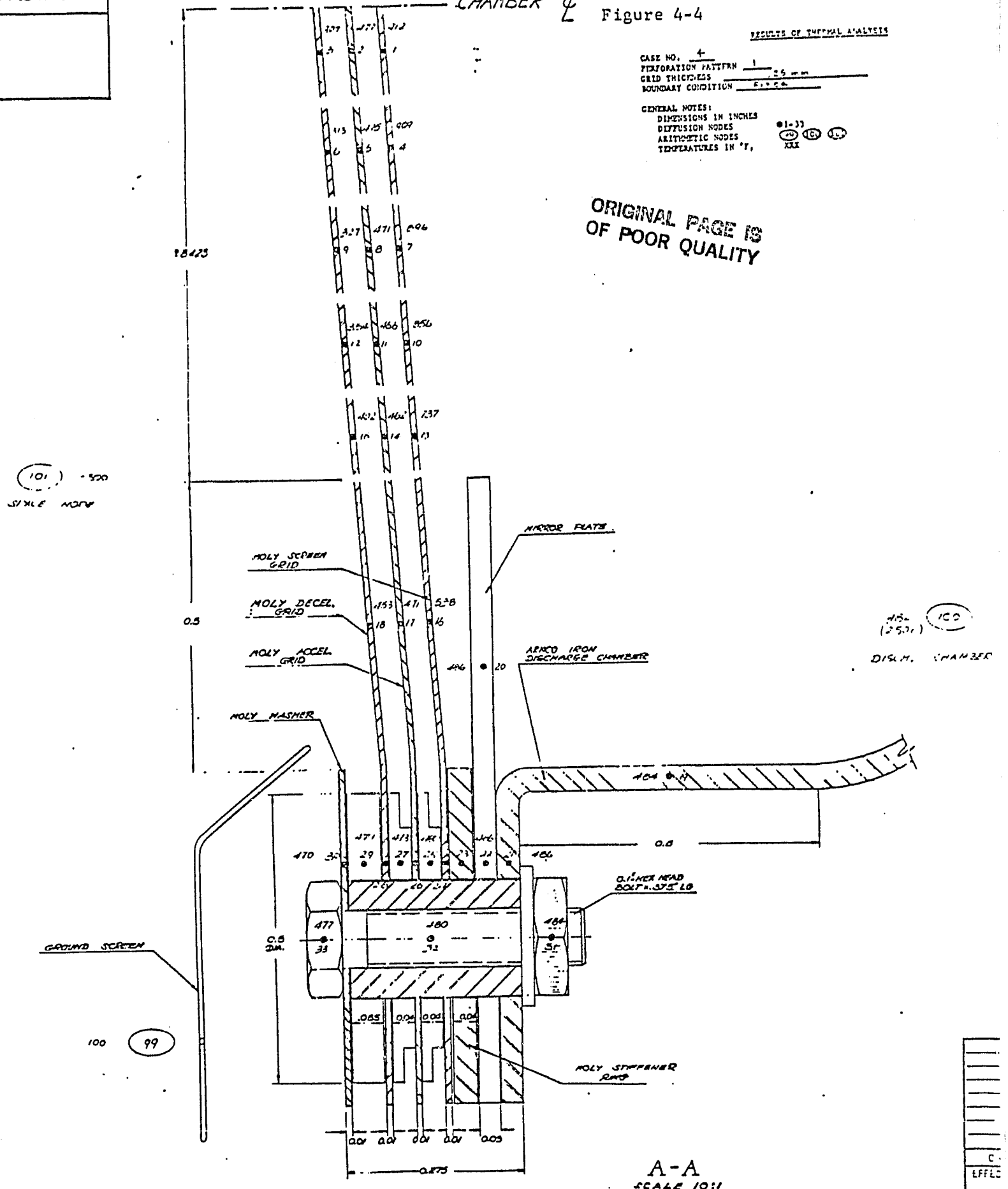

UNIT CLASSIFICATION

CHAMBER ℄

Figure 4-5

RESULTS OF THERMAL ANALYSIS

CASE NO. 5
PERFORATION PATTERN 1
GRID THICKNESS 0.5mm
BOUNDARY CONDITION Fixed

GENERAL NOTES:
DIMENSIONS IN INCHES
DIFFUSION NODES ●1-33
ARITHMETIC NODES (99) (100) (101)
TEMPERATURES IN °F, XXX



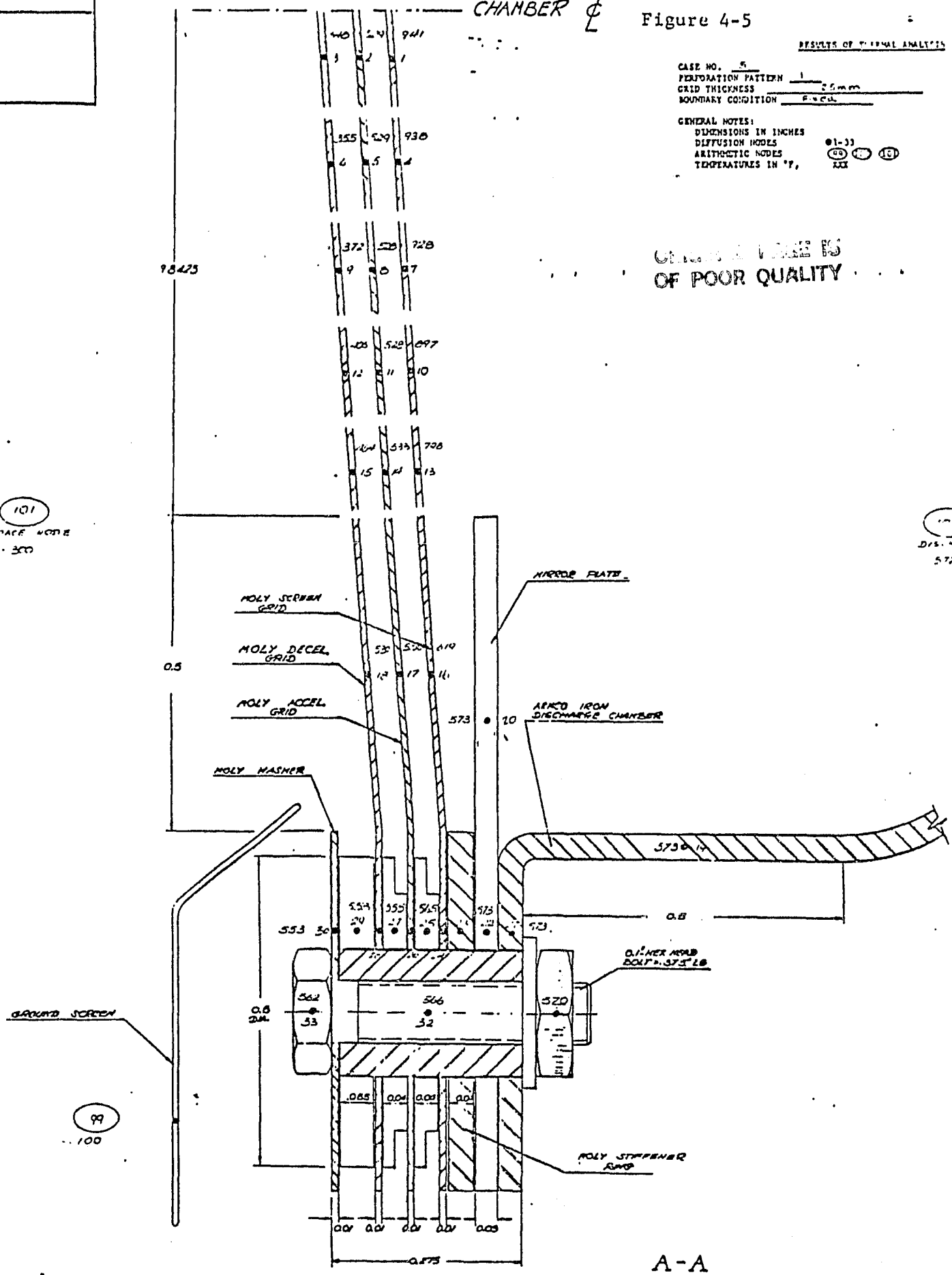


A-A
SCALE 10:1

Figure 4-6

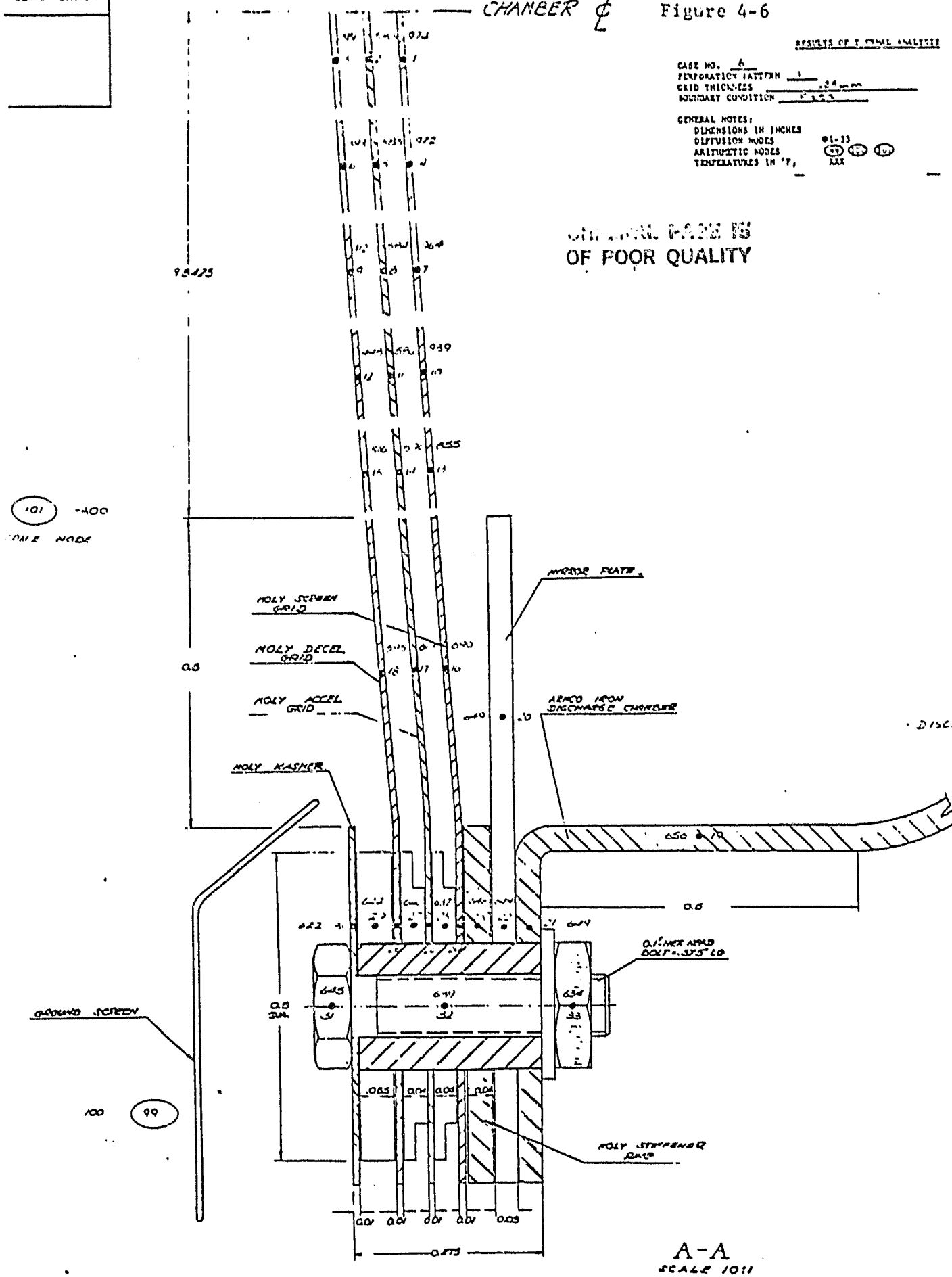
CHAMBER ℄
RESULTS OF THERMAL ANALYSIS
CASE NO. 6
PERFORATION PATTERN 1
GRID THICKNESS .04 mm
BOUNDARY CONDITION
GENERAL NOTES:
DIMENSIONS IN INCHES
DIFFUSION NODES
ARITHMETIC NODES
TEMPERATURES IN °F,
OF POOR QUALITY
101
-400
DATA NODE
MOLY SCREEN GRID
MOLY DECEL GRID
MOLY ACCEL GRID
MOLY WASHER
ARMCO IRON DISCHARGE CHAMBER
MOLY STIFFENER RING
GROUND SCREEN
100
99
0.5
0.6
A-A
SCALE 10:1

Figure 4-7

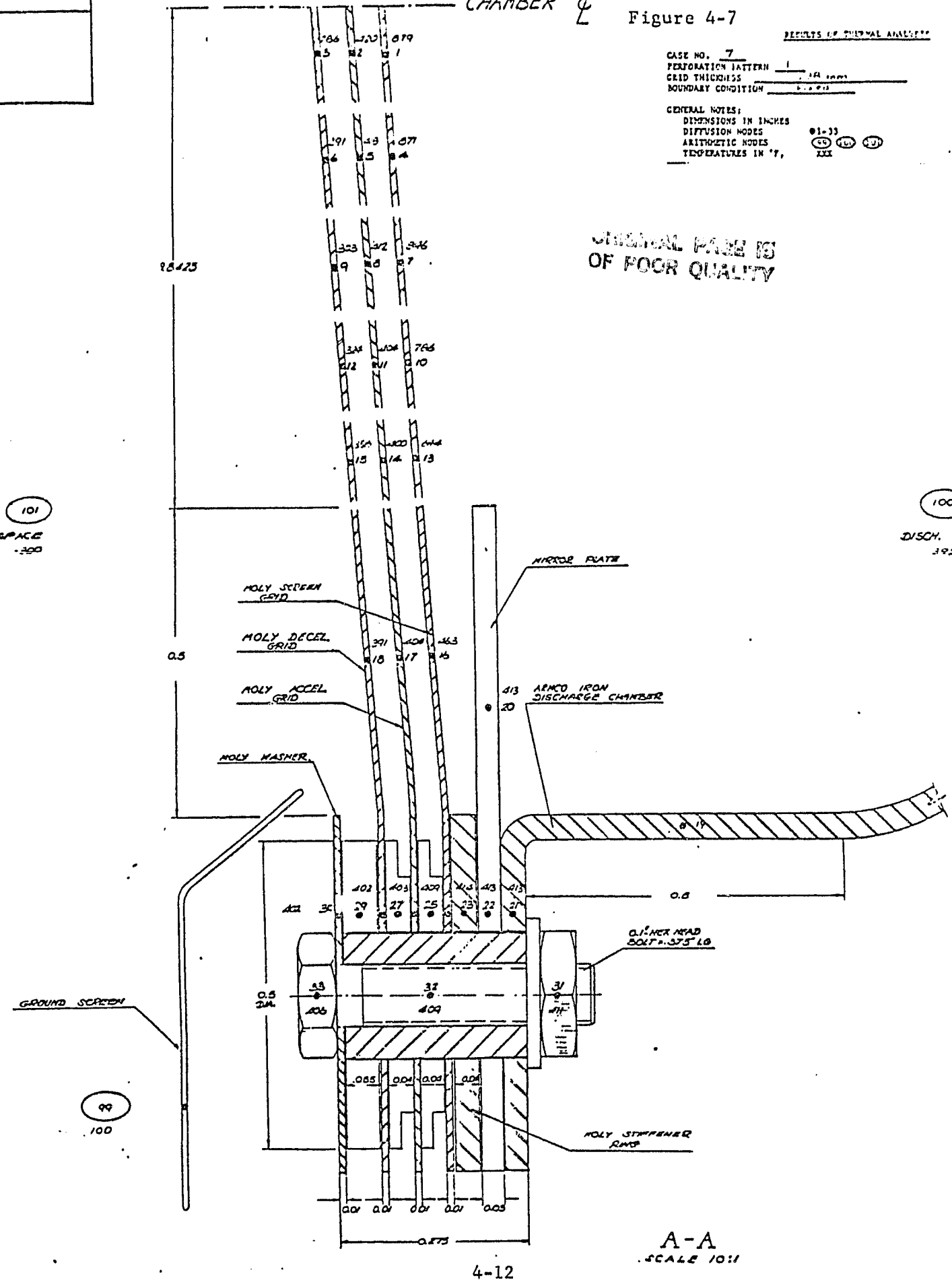
CHAMBER ℄
RESULTS OF THERMAL ANALYSIS
CASE NO. 7
PERFORATION PATTERN 1
GRID THICKNESS .18 inch
BOUNDARY CONDITION Given
GENERAL NOTES:
DIMENSIONS IN INCHES
DIFFUSION NODES 1-33
ARITHMETIC NODES 99 101 200
TEMPERATURES IN °F, XXX
ORIGINAL PAGE IS OF POOR QUALITY
.98423
0.5
101
SPACE
-300
100
DISCH. CHA
392
MIRROR PLATE
MOLY SCREEN GRID
MOLY DECEL. GRID
MOLY ACCEL. GRID
ARMCO IRON DISCHARGE CHAMBER
MOLY WASHER
0.6
0.1" PER HEAD BOLT = .375" LG
GROUND SCREEN
0.5 DIA.
99
100
MOLY STIFFENER RING
0.575
A-A
SCALE 10:1

SECURITY CLASSIFICATION

CHAMBER ℄ Figure 4-8

RESULTS OF THERMAL ANALYSIS

CASE NO. 8
PERFORATION PATTERN 1
GRID THICKNESS .11 mils
BOUNDARY CONDITION FLAT

GENERAL NOTES:
DIMENSIONS IN INCHES
DIFFUSION NODES ●1-33
ARITHMETIC NODES (1) (2) (3)
TEMPERATURES IN °F, XXX



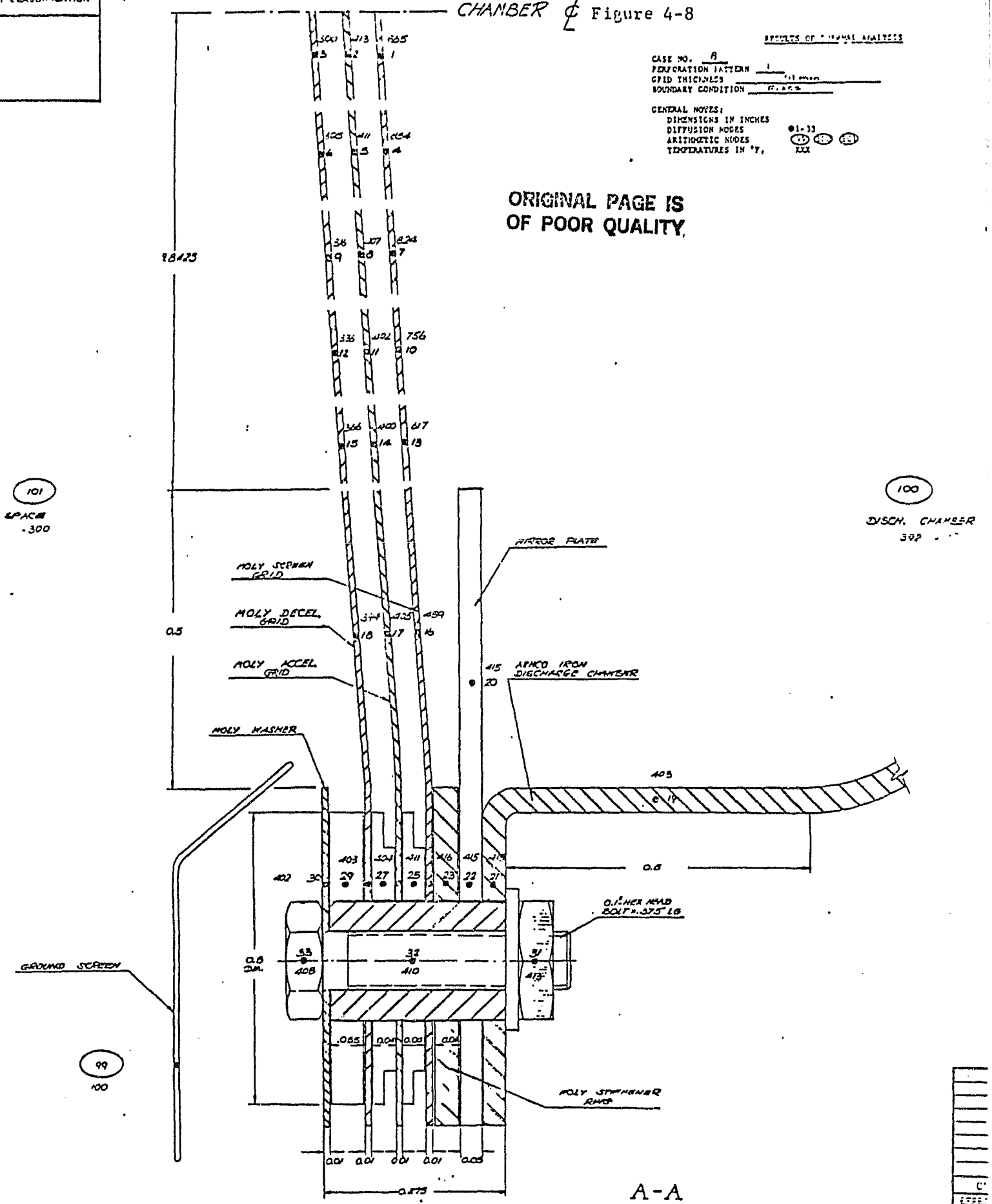


A-A
SCALE 10:1

SURITY CLASSIFICATION

Figure 4-9

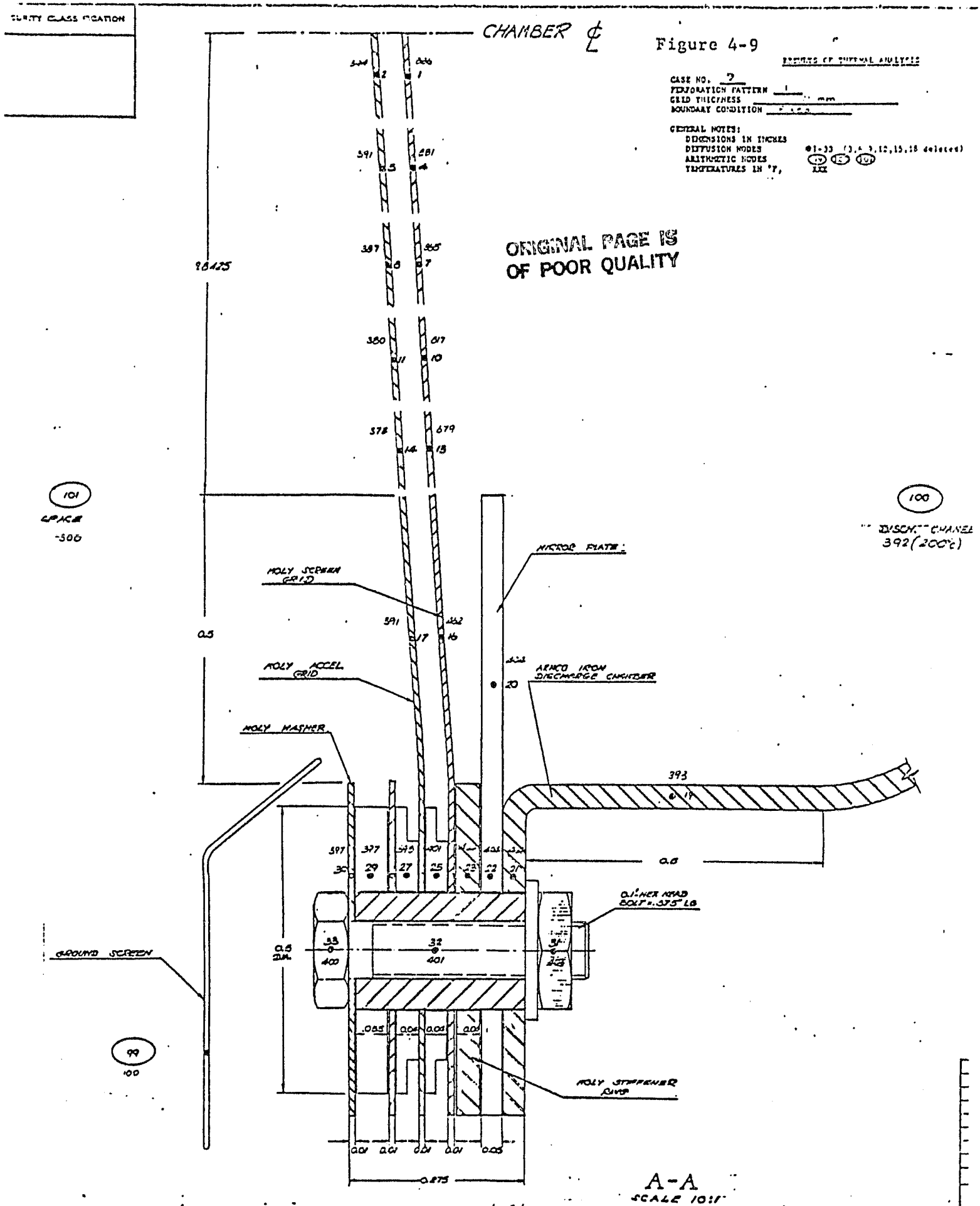

SECURITY CLASSIFICATION

CHAMBER ℄

Figure 4-10

RESULTS OF THERMAL ANALYSIS

CASE NO. 10
PERFORATION PATTERN 1
GRID THICKNESS 3.9 mm
BOUNDARY CONDITION WATER

GENERAL NOTES:
DIMENSIONS IN INCHES
DIFFUSION NODES @1-33 (3,6,9,12,15,18 deleted)
ARITHMETIC NODES (99) (100) (101)
TEMPERATURES IN °F, XXX



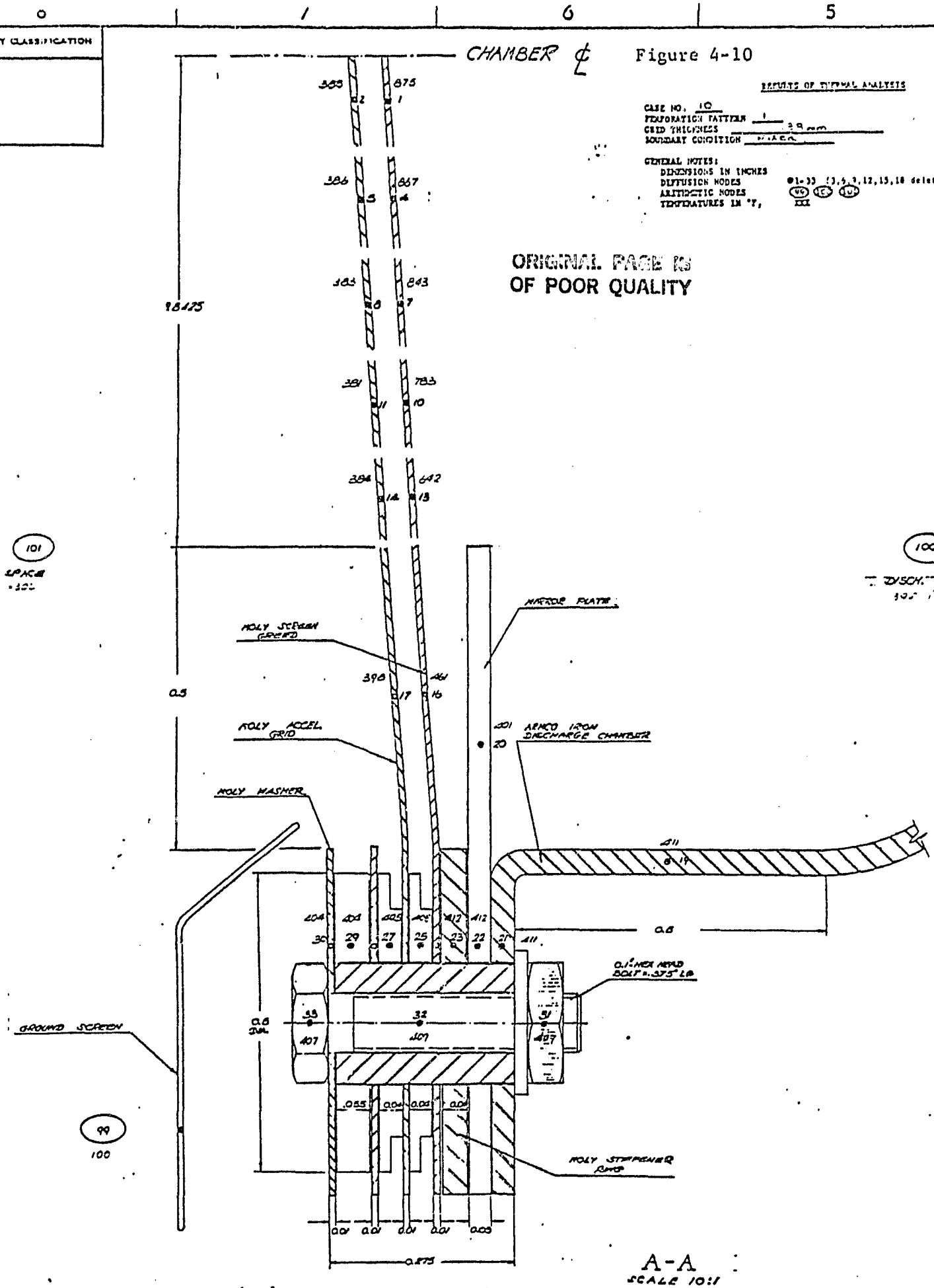


A-A
SCALE 10:1

Figure 4-11

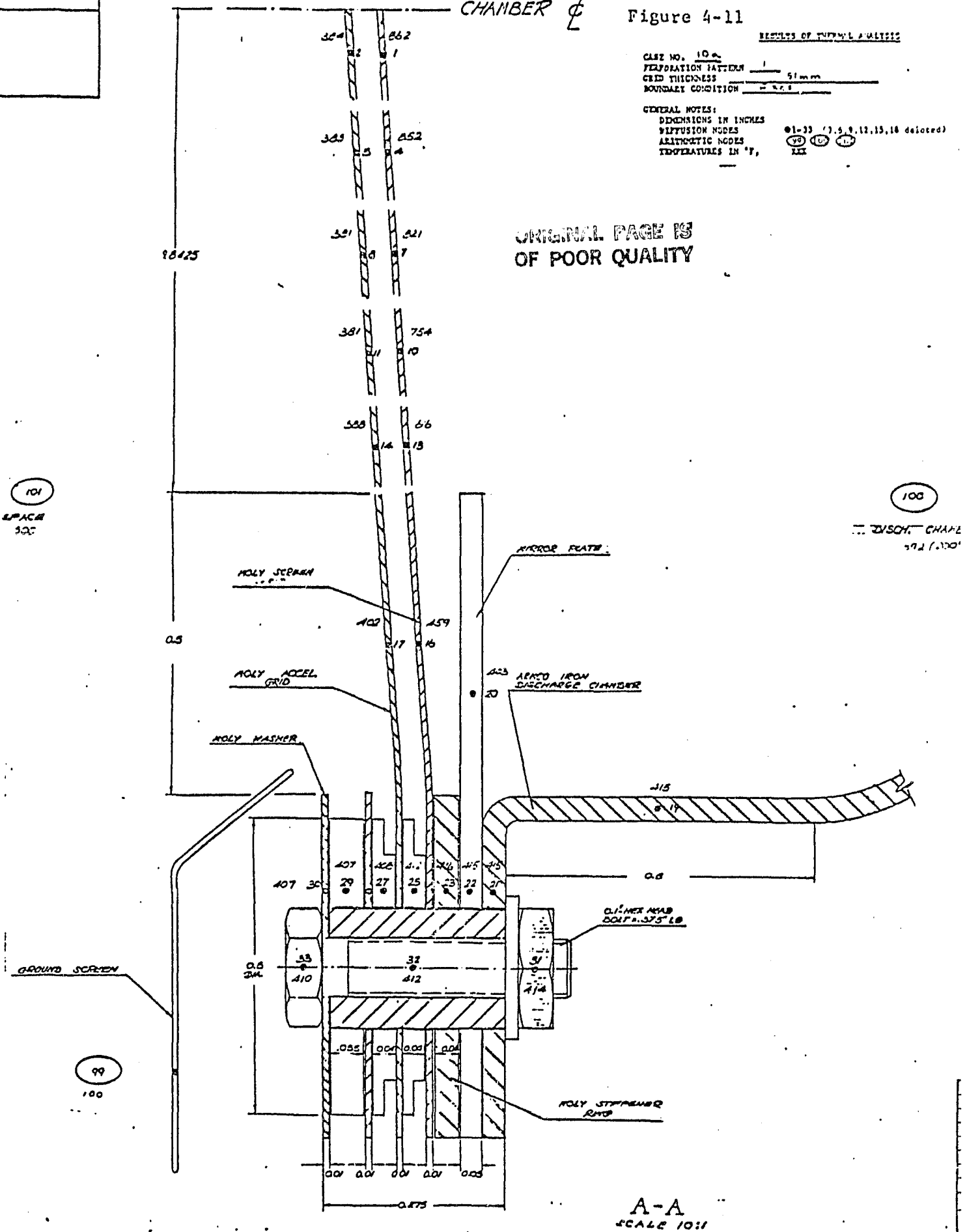
CHAMBER ℄
RESULTS OF THERMAL ANALYSIS
CASE NO. 10a
PERFORATION PATTERN 1
GRID THICKNESS 51mm
BOUNDARY CONDITION
GENERAL NOTES:
DIMENSIONS IN INCHES
DIFFUSION NODES ●1-33 (),5,9,12,15,18 deleted)
ARITHOETIC NODES
TEMPERATURES IN °F,
ORIGINAL PAGE IS
OF POOR QUALITY
MOLY SCREEN
MOLY ACCEL GRID
MOLY WASHER
GROUND SCREEN
MIRROR PLATE
ARMCO IRON DISCHARGE CHAMBER
CYLINDER HEAD BOLT
MOLY STIFFENER RING
A-A
SCALE 10:1

SECURITY CLASSIFICATION

CHAMBER ℄ Figure 4-12

RESULTS OF THERMAL ANALYSIS

CASE NO. 11
PERFORATION PATTERN 1
GRID THICKNESS Screen .38 mm / Accel .89 mm
BOUNDARY CONDITION Case 2

GENERAL NOTES:
DIMENSIONS IN INCHES
DIFFUSION NODES ●1-33 (3,6,9,12,15,18 deleted)
ARITHMETIC NODES (99) (100) (101)
TEMPERATURES IN °F, XXX



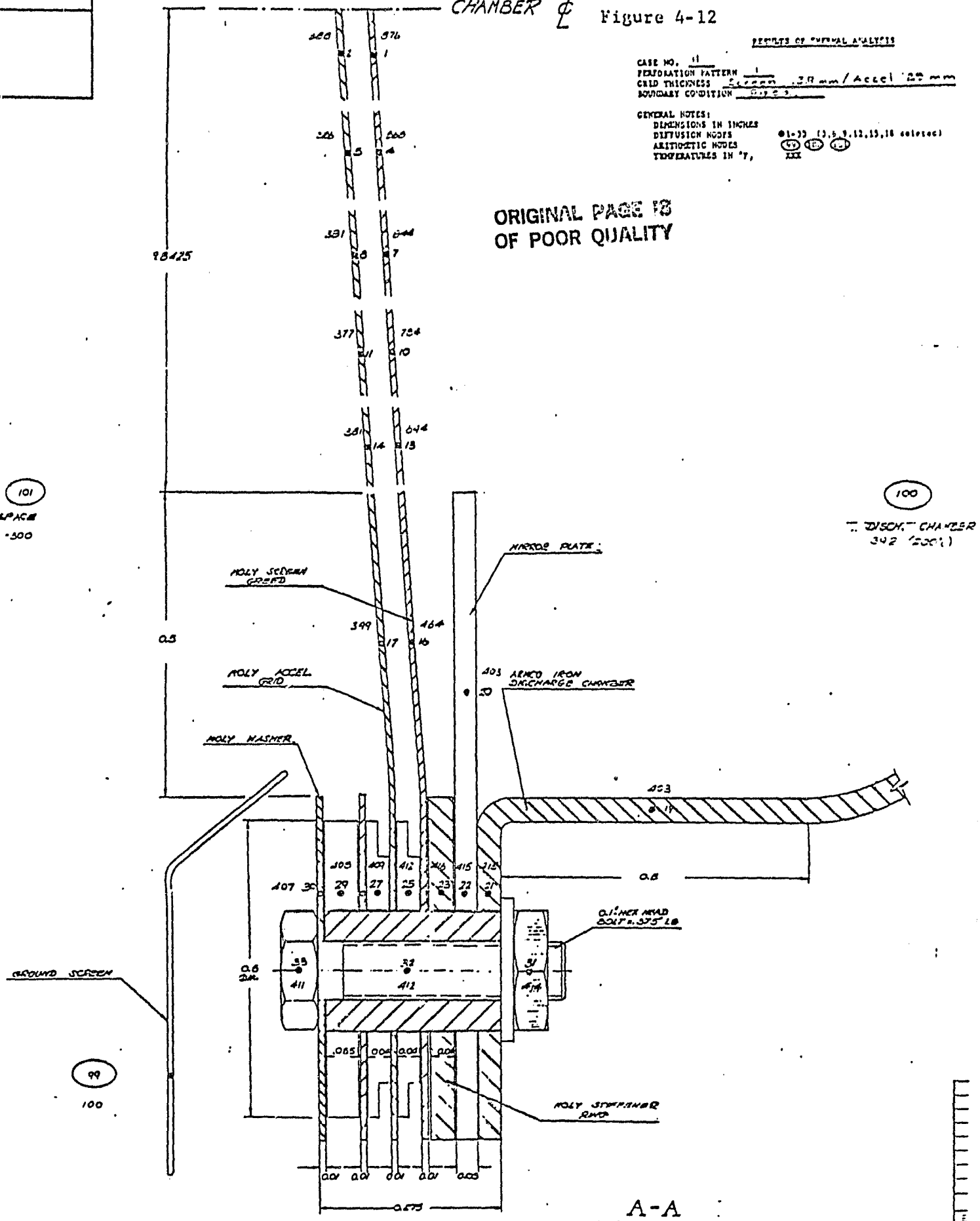


A-A
SCALE 10:1

CHANGER ℄ Figure 4-13

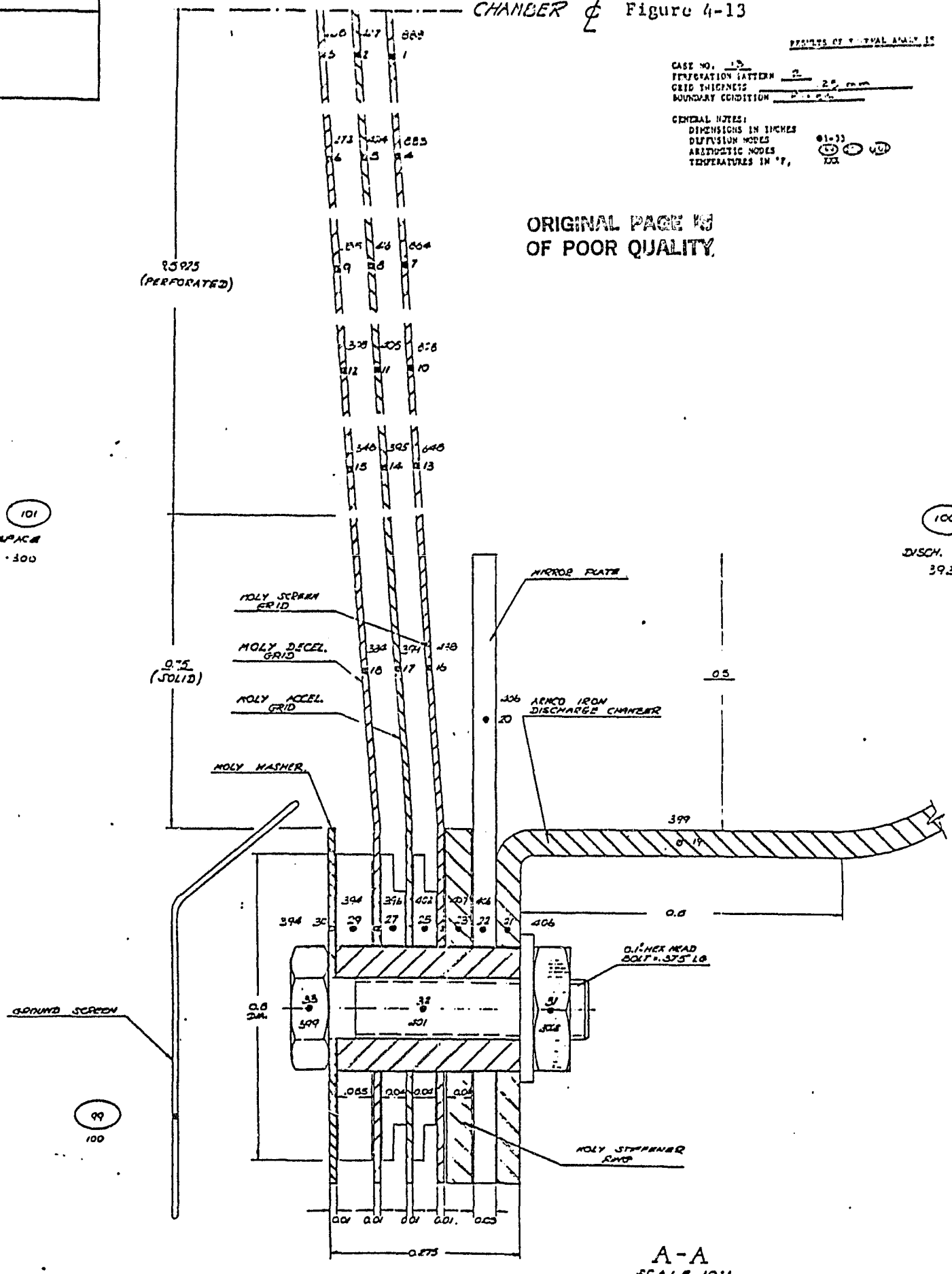

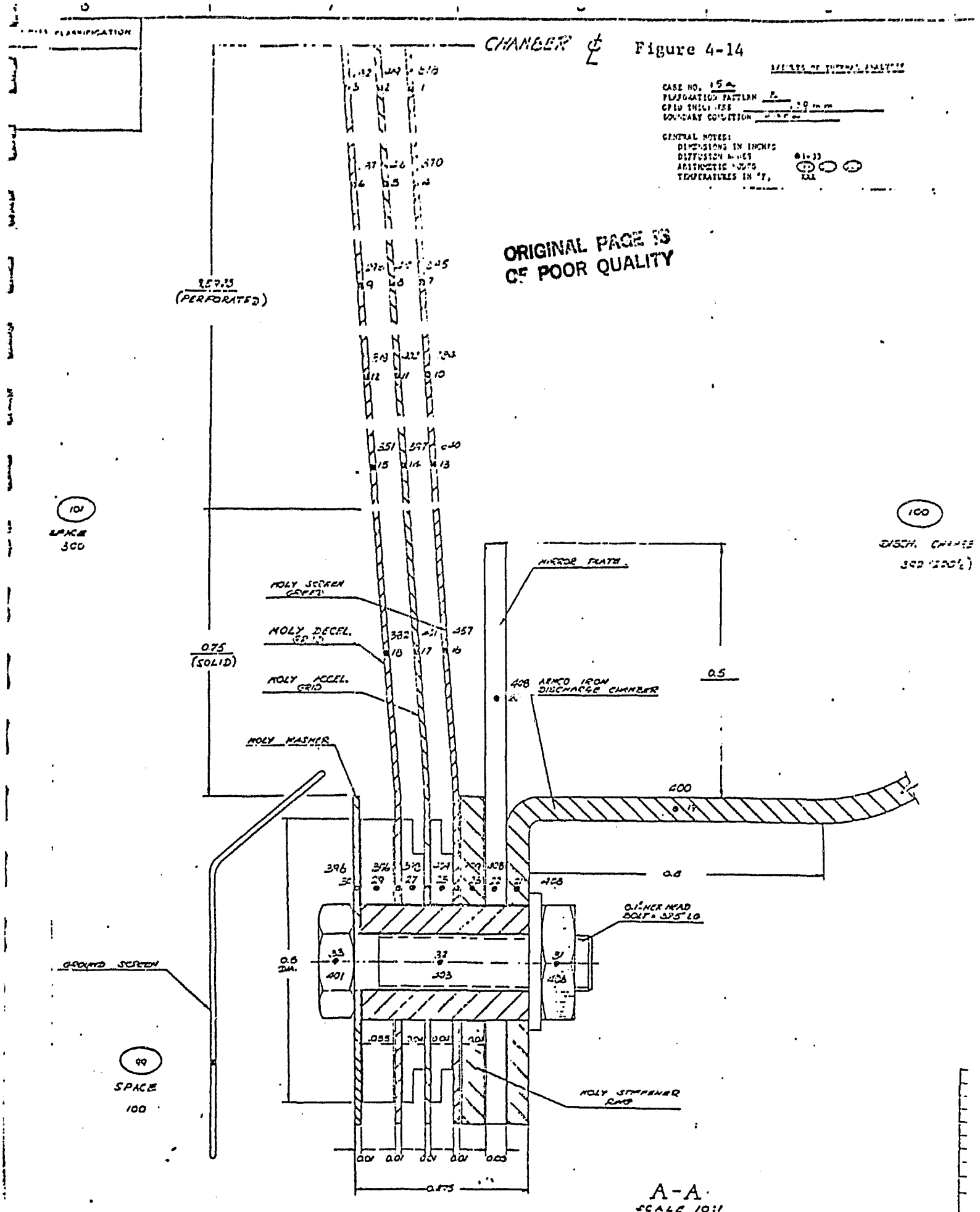


ORIGINAL PAGE IS OF POOR QUALITY

Figure 4-14

CHAMBER ℄

Figure 4-15

RESULTS OF 2 D THERMAL ANALYSIS

CASE NO. 17
PERFORATION PATTERN 2
GRID THICKNESS .5 mm
BOUNDARY CONDITION ADIA

GENERAL NOTES:
DIMENSIONS IN INCHES
DIFFUSION NODES ●1-37
ARITHOTIC NODES ⊗ ⊕ ⊗
TEMPERATURES IN °F, XXX



.5925
(APPROXIMATED)

101
SPACE
-300

100
DISCH. CH-
392

MIRROR PLATE

MOLY SCREEN GRID

MOLY DECEL. GRID

MOLY ACCEL. GRID

.975
(SOLID)

.50

ARMCO IRON DISCHARGE CHAMBER

MOLY WASHER

.376

0.8

OVERHEAD BOLT ø.375" LG

GROUND SCREEN

0.5 DIA.

MOLY STIFFENER ROD

99
100

0.775

A-A
SCALE 10:1

## 4.2 OPTICS STRUCTURAL ANALYSIS

### 4.2.1 ANALYTICAL APPROACH

The CDC Stardyne Structural Analysis System was used for the structural computations. An elastic, finite element structural model was constructed to compute deflections and stresses generated by the temperatures predicted in subsection 4.1. The model of the ion engine was simplified by modeling one quadrant; i.e., possibly by simulating slopes and direction of movements at the boundaries to simulate boundary conditions. The grids and discharge chamber are modeled with quadrilateral and triangular plates. Circular beams are used for the attachment screws. Figures 4-16 and 4-17 illustrate the model. Small deflection theory is assumed for the analysis. The structural model was made analogous to the thermal model for ready input of nodal temperatures.

The elastic constants, namely the Young's modulus and Poisson's ratio, have been evaluated for both perforated and unperforated material. Modifying the elastic constants to account for grid perforation has been shown to have no measurable effect upon thermal deformations, a result supported by a study by Hughes Aircraft Company on the LeRC/Hughes J-series thruster. Stress concentration factors from O'Donnell and Langer were used to calculate peak stresses around the perforations with a maximum concentration $K_t = 8$. The structural material properties utilized in the analysis were standard handbook properties for the applicable materials.

Although it may seem contradictory, the "fixed boundary" thermal analysis results were utilized in the "free boundary" structural analysis. This thermal analysis assumes no contact at the joint whatever as discussed in subsection 4.1. Since contact increases the grid thermal gradient, and hence the stress levels, the "fixed boundary" temperatures were used to ensure a conservative analysis.

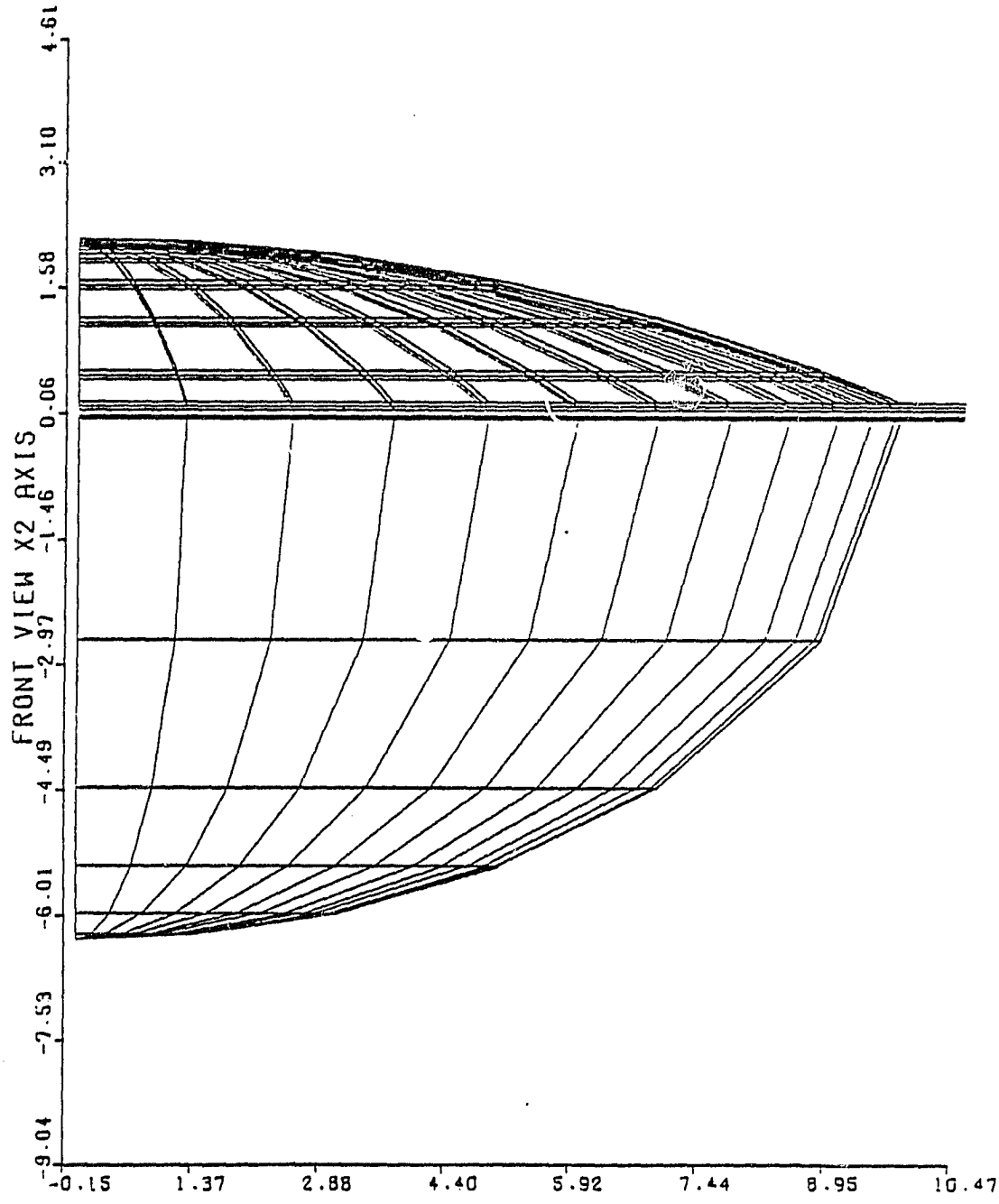


65907

Figure 4-16. Structural Model

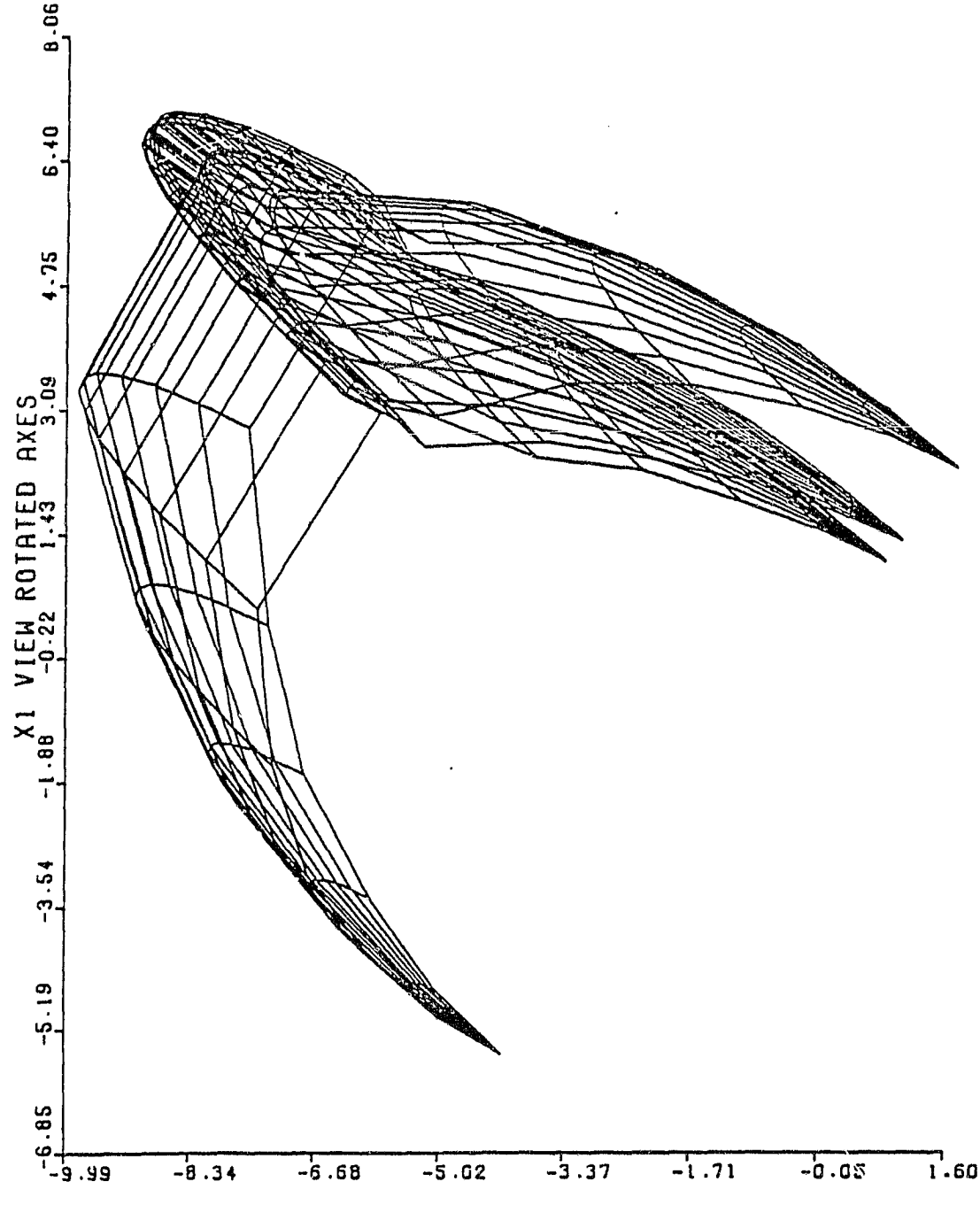


65881

Figure 4-17. Thermal Model

### 4.2.2 DISCUSSION OF RESULTS

The cases analyzed are listed in table 4-1, and the results from the structural analysis are summarized in table 4-2. The general conclusions that may be drawn from the calculations are as follows:

a. Increasing the discharge chamber temperature increases the stress in the grids but improves the grid gap uniformity only slightly.

b. Increasing the grid thickness reduces the grid stress but improves the grid gap uniformity only slightly.

c. Removing the decelerator grid does not seem to pay dividends in either grid stress levels or deflections.

d. Allowing the optics assembly to slip at the attachment of the discharge chamber greatly reduces the grid stress levels without penalizing the deflections significantly.

e. Increasing the radius of curvature of the grids above 65 cm causes a significant penalty in both stress and deflections. The crossover can be eliminated by proper initial contours in the cold condition, or by moving the decelerator grid farther outboard. However, the ability of the engine to operate at partial power may be impaired.

f. In only one case (11a) is the yield strength of molybdenum exceeded.

Figures 4-18 through 4-20 further illuminate the condition of the grids at full power for Cases 5, 15A, and 15B, respectively. The stresses and deflections are shown at several radial locations for the three grids.

## 4.3 DISCHARGE CHAMBER THERMAL ANALYSIS

A preliminary analysis of the ion engine indicated that it is capable of radiating to space less than 40 percent of the expected 4500 watt power dissipation of the discharge chamber if operated at a uniform 350°C, the upper limit of acceptable temperatures. Hence, it is

TABLE 4-2

SUMMARY OF RESULTS FROM STRUCTURAL ANALYSIS

| CASE | DECEL STRESS PSI | ACCEL STRESS PSI | SCREEN STRESS PSI | YIELD STRENGTH PSI | ROOM TEMP GAP-IN. | ACCEL/ DECEL GAP-IN. | ACCEL/ SCREEN GAP-IN. | COMMENTS |
|---|---|---|---|---|---|---|---|---|
| 1 | 30,352 | 32,509 | 42,840 | 60,000 | .04 | .0293 | .0089 | |
| 4 | 37,716 | 40,310 | 49,420 | ↓ | ↓ | .0287 | .0107 | |
| 5 | 45,696 | 51,984 | 56,476 | | | .0280 | .0125 | |
| 7 | 28,420 | 30,044 | 37,940 | | | .0311 | .0091 | |
| 8 | 26,558 | 20,910 | 34,160 | | | .0325 | .0095 | |
| 9 | -- | 41,934 | 52,136 | | | -- | .00651 | |
| 11a | -- | 39,904 | 83,244 | | | -- | TOUCHING .0083 CROSSOVER | |
| 11b | -- | 37,613 | 43,540 | | | -- | TOUCHING .0074 CROSSOVER | |
| 12 | 688 | 194 | 13,597 | | | .0308 | .0086 | |
| 13 | 815 | 319 | 14,196 | | | .0291 | .0086 | |
| 14 | 30,296 | 32,422 | 46,200 | | | .0293 | .0090 | |
| 15a | 1,673 | 275 | 19,289 | | | .0178 | TOUCHING .0325 CROSSOVER | |
| 15b | 21,358 | 23,766 | 16,924 | | | .0183 | TOUCHING .0308 CROSSOVER | |
| 16 | 21,308 | 17,210 | 41,244 | | | .0118 | TOUCHING .0599 CROSSOVER | |

65910

ORIGINAL PAGE IS
OF POOR QUALITY

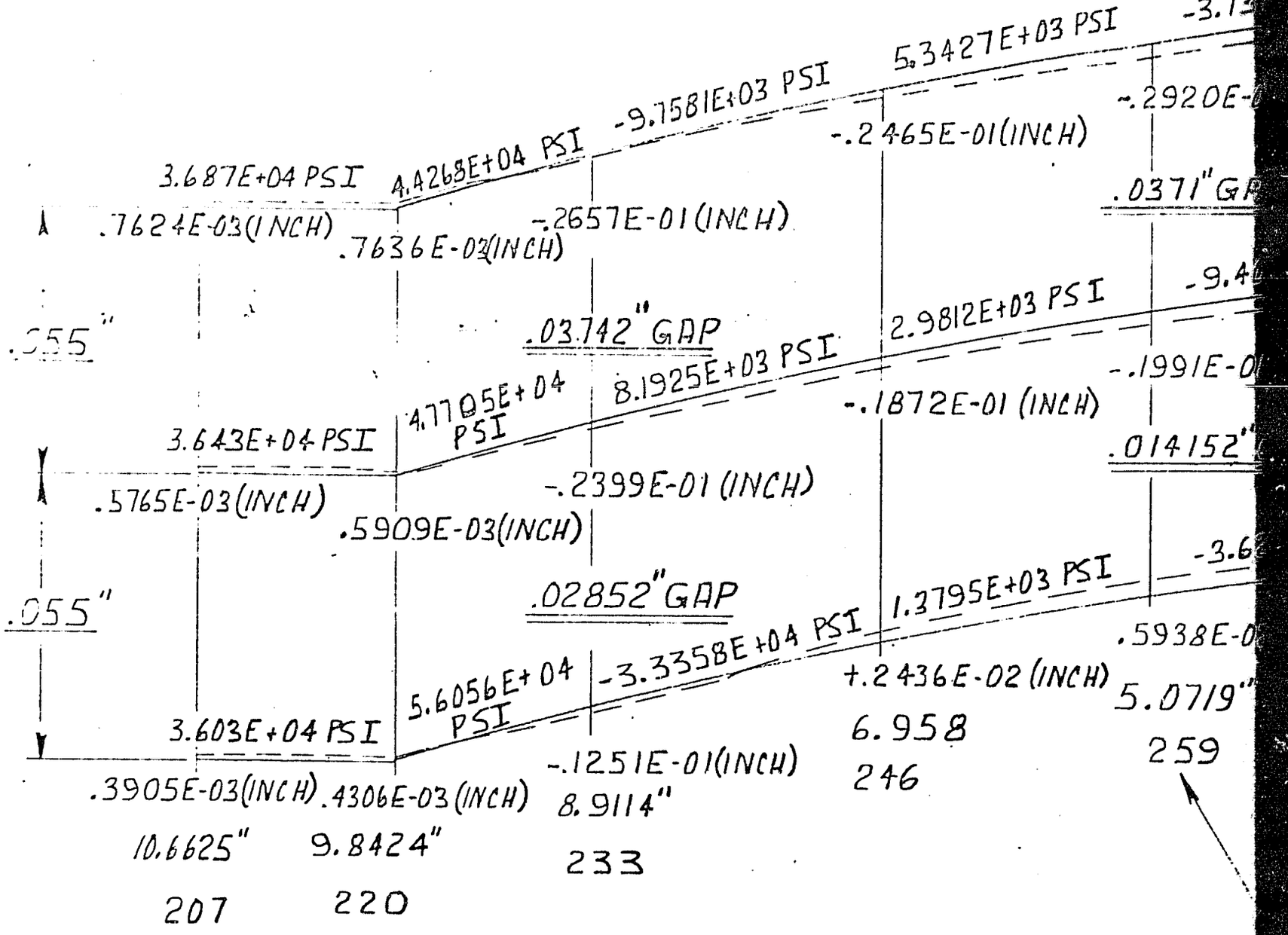


FOLDOUT FRAME

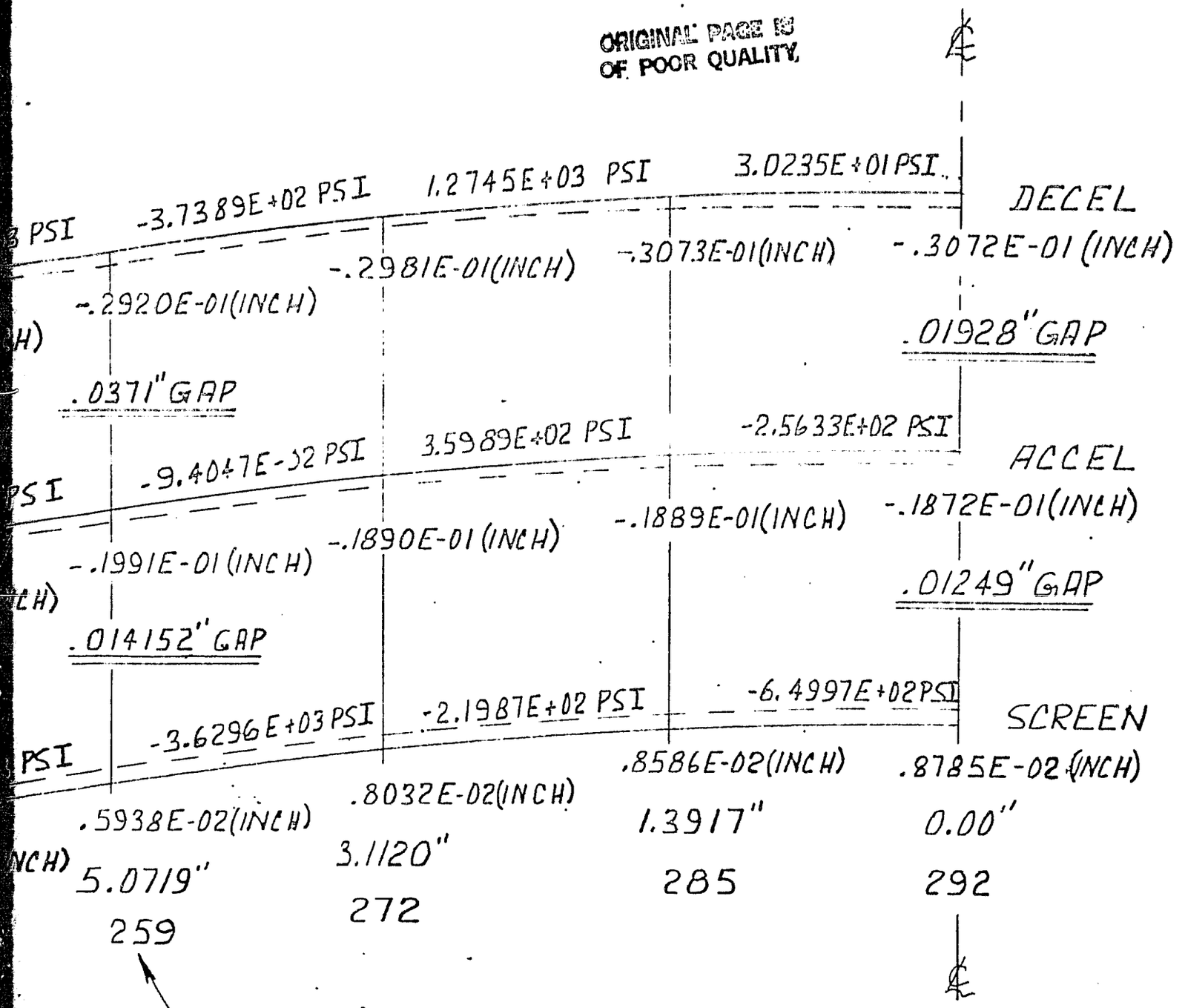


Figure 4-18. Stress Levels and Deflections in Ion Engine Optics Assembly Case 5

ORIGINAL PAGE IS
OF POOR QUALITY

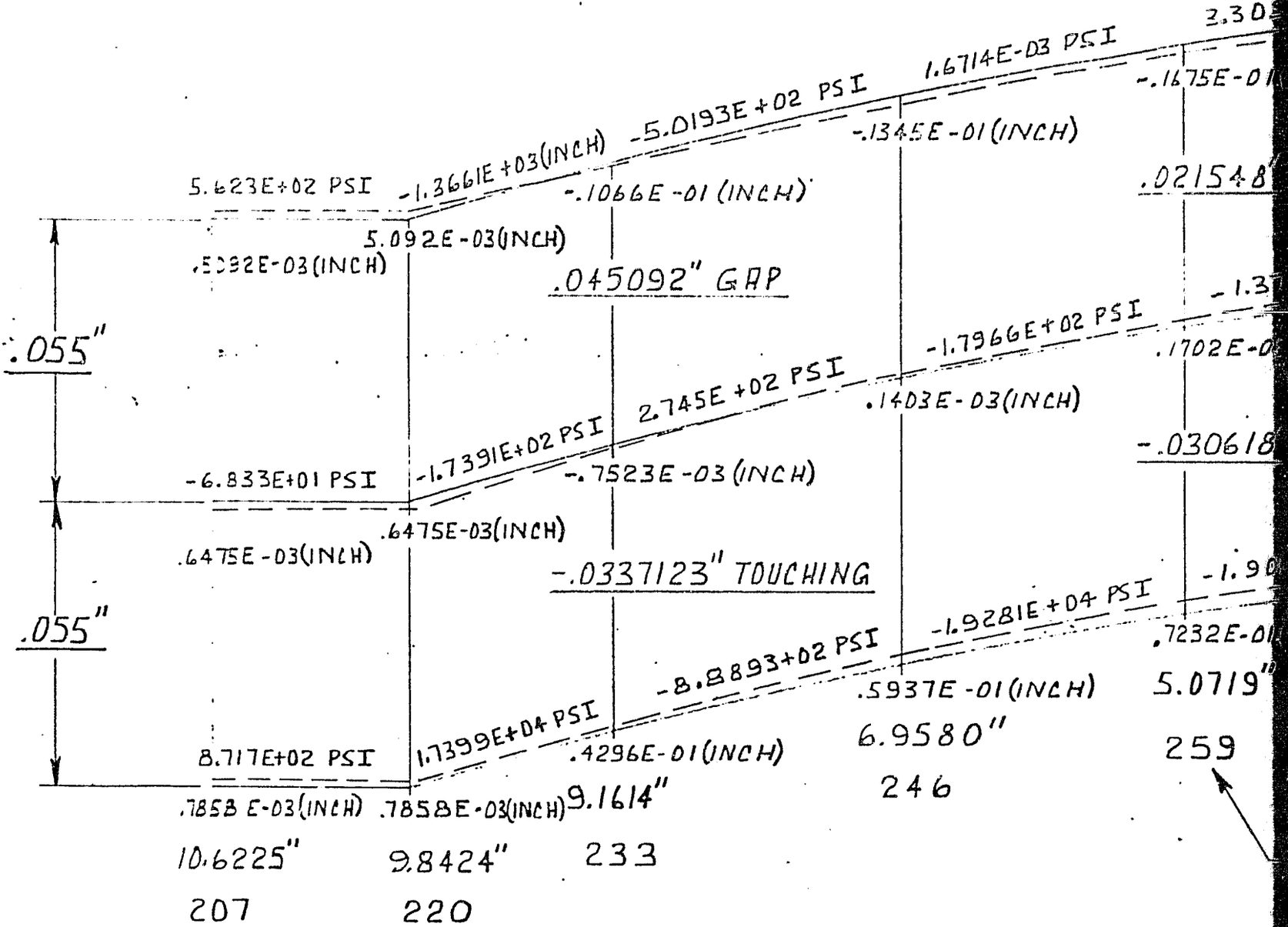


FOLDOUT FRAME

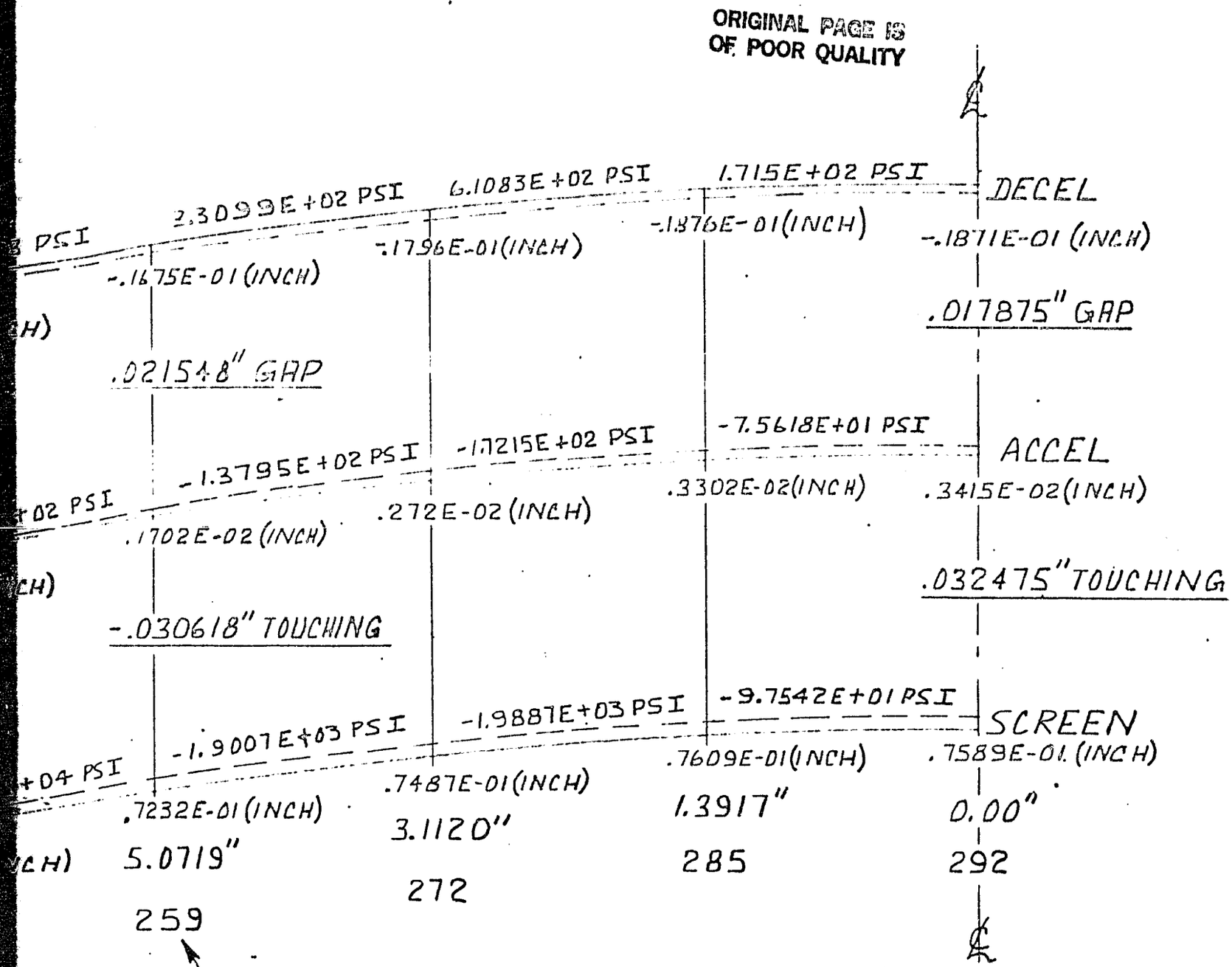




Figure 4-19. Stress Levels and Deflections in Ion Engine Optics Assembly Case 15B

2 FOLDOUT FRAME

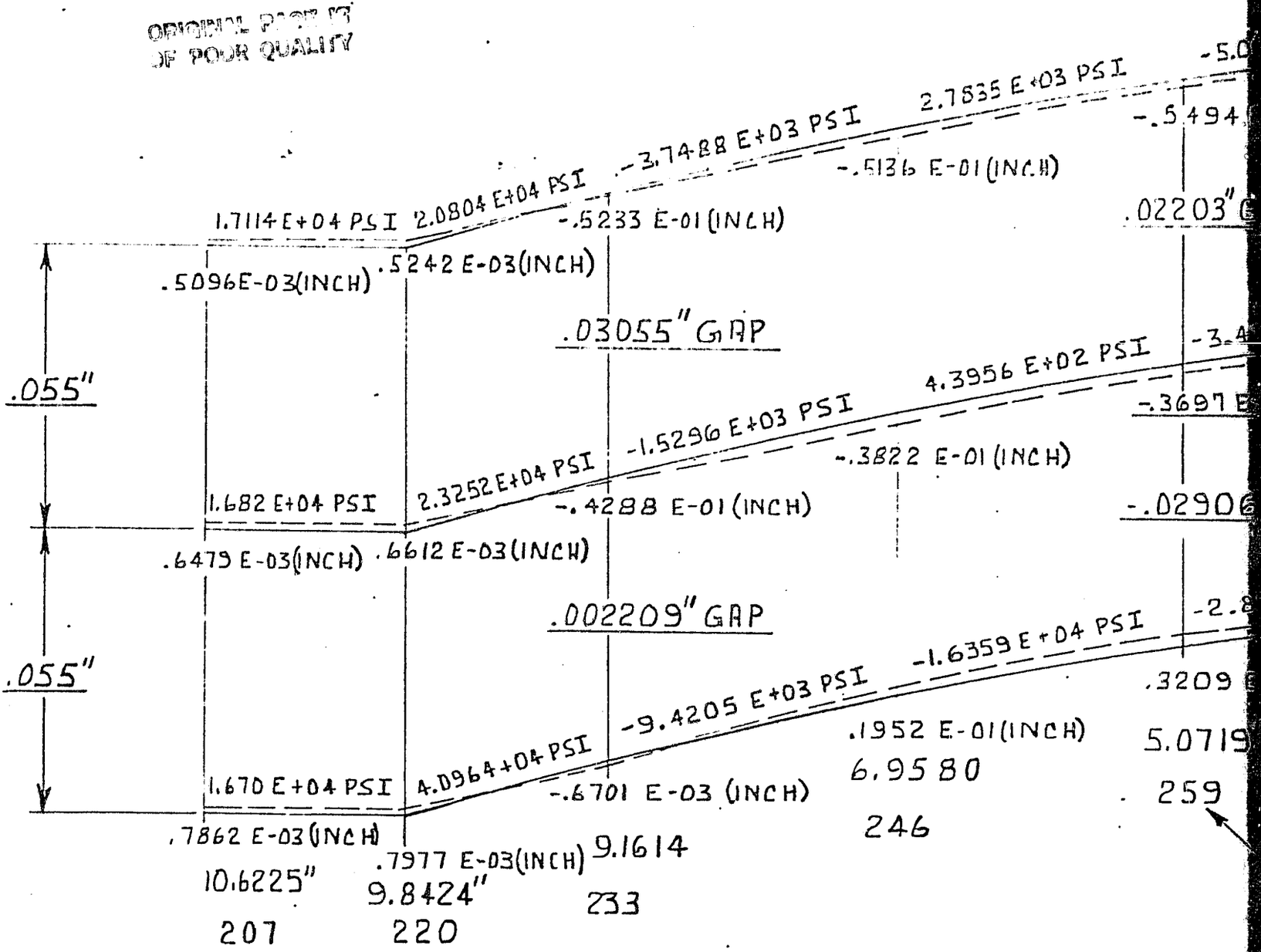


FOLDOUT FRAME

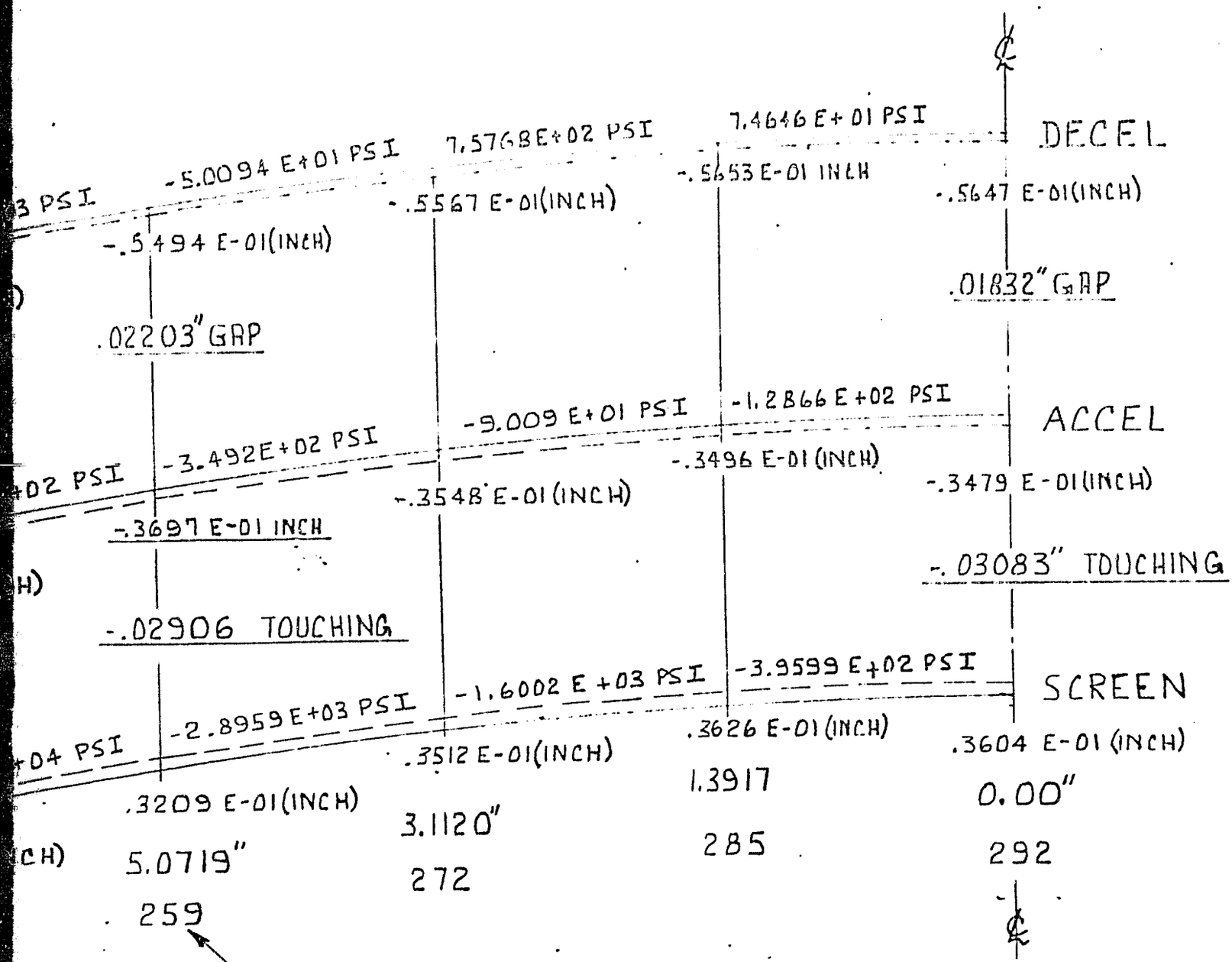




Figure 4-20. Stress Levels and Deflections in Ion Engine Optics Assembly Case 15A

2 FOLDOUT FRAME

necessary to find a method to enhance heat removal from the engine. Because of the criticality of grid stress, alignment and deformation due to thermal expansion, the cooling system must be capable of minimizing thermal gradients in the discharge chamber. For the periodic magnet geometry selected, the heat will arrive at the thruster chamber walls in three ways. Ions will impinge on the anode strips which will in turn conduct and radiate to the walls and the plasma will radiate directly to walls, magnets, anode strips, and screen.

Three possible methods of heat removal are:

a. A conduction design with increased outer area for space radiation
b. One or more heat pipes
c. Active cooling loop

A brief analysis of a conduction scheme indicated that, to maintain uniform temperatures, it would be excessively heavy and complex. Unfortunately, time did not permit a proper analysis of heat pipes, but it can be said that they will be necessarily complex and that extensive development costs will be incurred.

Of the three methods, the most advisable approach would seem to be an active cooling loop. The technology is well developed from the Apollo and Space Shuttle programs. This approach will allow concentration of the development on the ion engine without diluting the effort for cooling system development.

The system will use a liquid coolant and will include a pump, reservoir, accumulator, space radiator, and cooling coils on the discharge chamber. It must also be thermostatically controlled to provide a

predetermined temperature on the discharge chamber. Care will be exercised in the cooling coil design and inlet manifolding to achieve uniform cooling of the chamber. A fluid that has a high dielectric strength will be used to electrically isolate the cooling system (for example, Fluorinert FC-75, dielectric strength at 25°C = 55 kV per 2.5 mm).

# SECTION 5

# CONCEPTUAL DESIGN

The results of the studies detailed in Sections 2, 3, and 4 were combined to generate a conceptual design of a 50 cm diameter inert gas ion thruster. This concept includes all thruster components such as a neutralizer but does not include propellant delivery components for flow control or high voltage isolation. For this study, such items are considered part of the propellant delivery system.

The thruster design is based on an oblate spheroid discharge chamber spun from soft iron. Figure 5-1 is a section along the thrust axis. This view shows the relative locations of the three grid ion optics, boundary anodes, magnets, and external cooling coils. A single, center cathode assembly provides ionizing electrons. This assembly includes the keeper and baffle supports and is handled as a unit for experimental flexibility. The cathode assembly is surrounded by an annular permanent magnet that trims the axial magnetic field as well as completing the boundary magnetic circuit. No magnetic baffle is anticipated.

The neutralizer assembly is a plasma bridge device similar to the main cathode and is mounted to the main support ring just outboard of the discharge chamber as can be seen in figure 5-2. The cooling coils and cathode support bracket are shown in another view in figure 5-3.

One of the advantages of this design is the ease with which the discharge chamber can be lengthened for investigation of mean free path

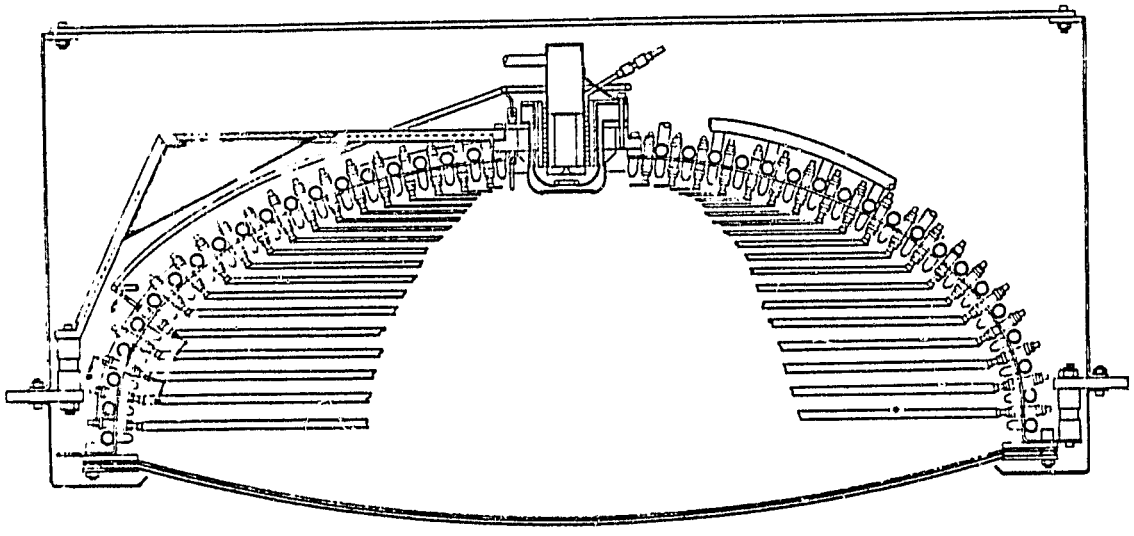

65919

Side View

Figure 5-1. 50 cm Thruster Conceptual Design

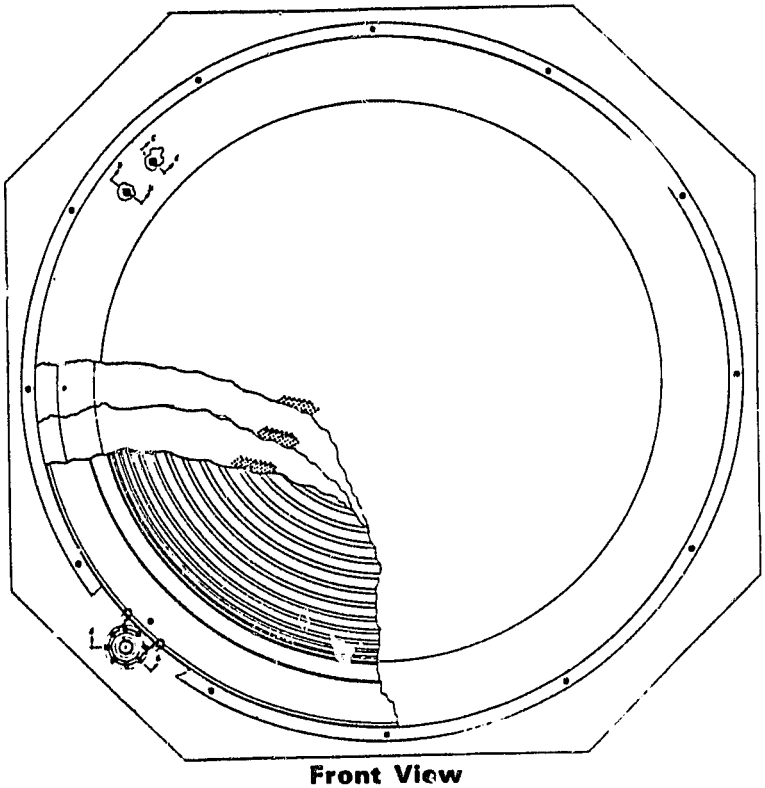

Front View

Figure 5-2. 50 cm Thruster Conceptual Design

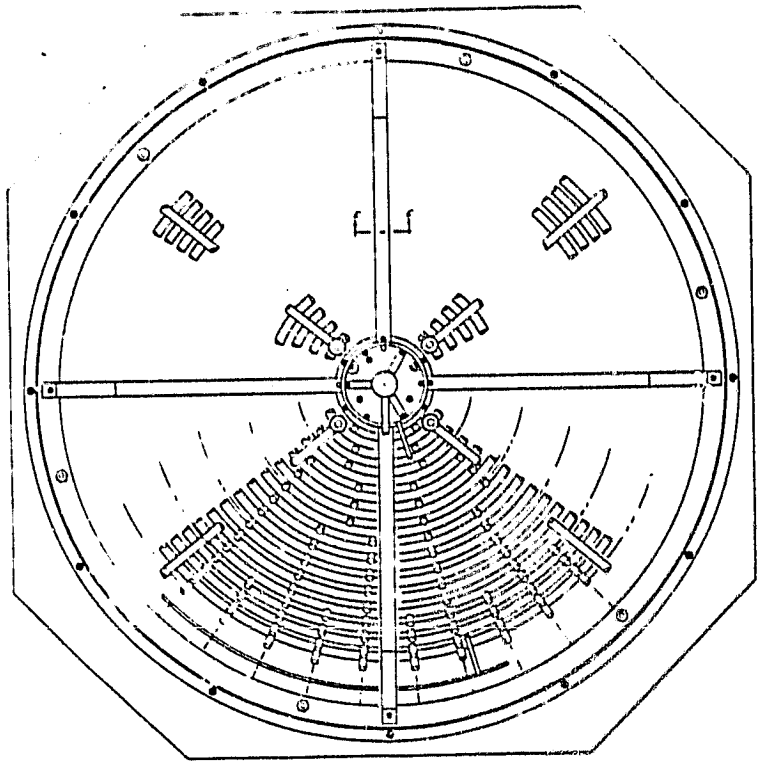


65913

Figure 5-3. Thruster Conceptual Design

effects for various propellants. Figures 5-4 and 5-5 show a similar design in the 12 cm size with the second figure having two 2.5 cm extensions added.

The thruster concept developed during this effort will provide the increased thrust and performance that are envisioned for the large space system mission now being planned. This design provides new highs in thruster power density and thrust-to-power ratios. A summary of projected performance is given in table 5-1.

TABLE 5-1

PROJECTED LARGE THRUSTER PARAMETERS

| | Argon | Xenon |
|---|---|---|
| Thrust, Newtons | 0.5 | 0.5 |
| Specific Impulse, seconds | 6076 | 3530 |
| Net Accelerating Potential, volts | 1000 | 1000 |
| Net Ion Beam Current, amperes | 17.2 | 9.5 |
| Ion Beam Power, kilowatts | 17.2 | 9.5 |
| Electrical Efficiency, percent | 0.80 | 0.87 |
| Mass Efficiency, percent | 0.86 | 0.91 |
| Total Efficiency, percent | 0.69 | 0.79 |
| Ion Beam Current Density, $A/cm^2$ | 0.009 | 0.005 |
| Discharge Chamber Efficiency, eV/ion | 240 | 145 |
| Discharge Power, kilowatts | 4.1 | 1.4 |
| Discharge Voltage, volts | 50 | 40 |
| Discharge Current, amperes | 83 | 54 |
| Keeper Power, kilowatts | 0.1 | 0.1 |
| Keeper Voltage, volts | 13 | 11 |
| Keeper Current, amperes | 10 | 5 |
| Total Power, kilowatts | 21.4 | 11.0 |
| Thrust-to-Power Ratio, Newton/kW | 0.023 | 0.043 |

ORIGINAL PAGE
BLACK AND WHITE PHOTOGRAPH

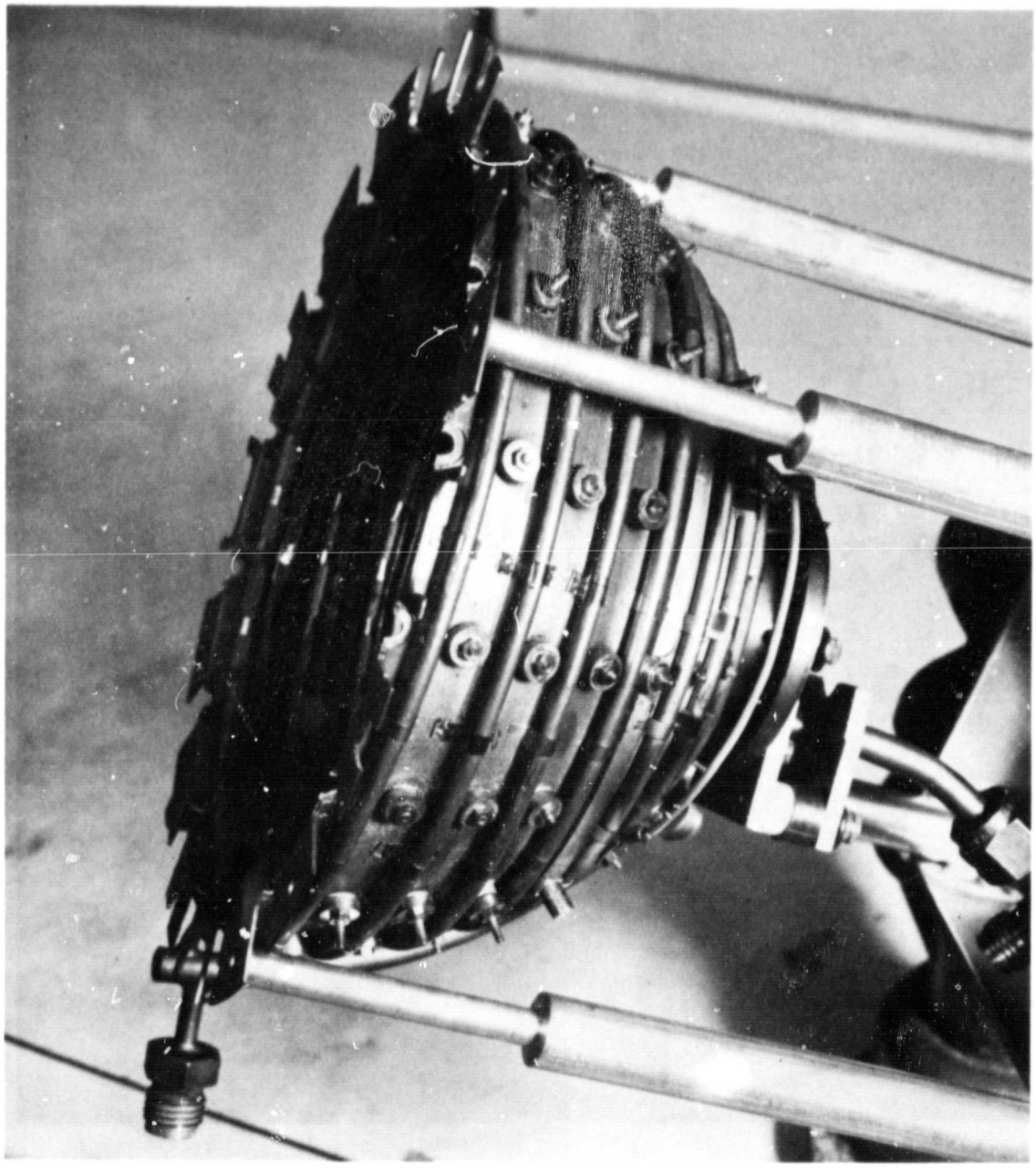

38054

Figure 5-4. 12 cm Hemispherical Inert Gas Ion Thruster

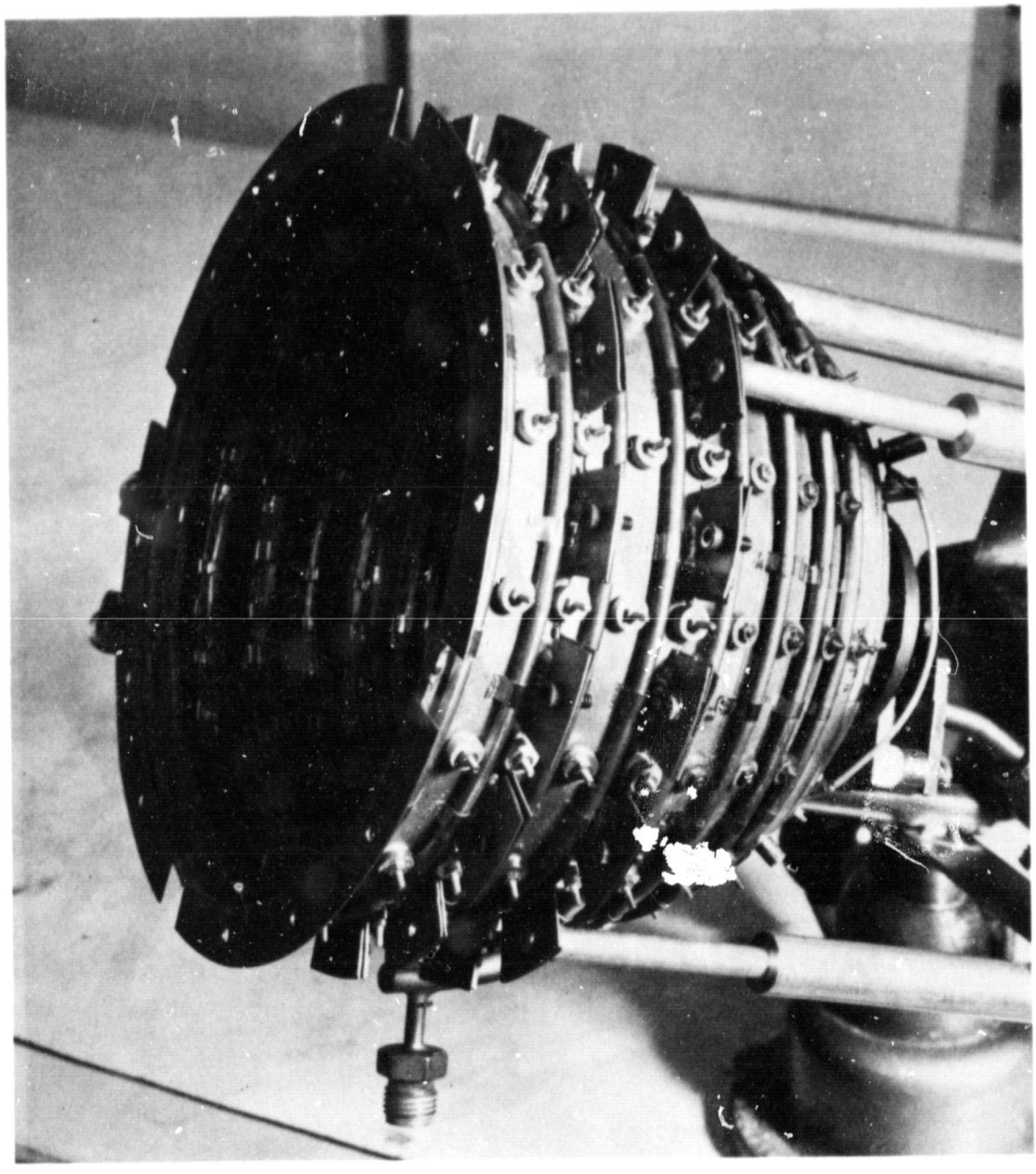

38052

Figure 5-5. 12 cm Hemispherical Thruster with Two Chamber Extension Units

# SECTION 6

# POWER MANAGEMENT AND CONTROL REQUIREMENTS

This section identifies the minimum power management and control requirements (PMaC) needed to operate the 50 cm inert gas thruster conceptually designed during this program.

## 6.1 CONTROL ALGORITHMS

For effective operation the PMaC must provide some autonomous response to off-normal conditions. The following algorithms are the minimum required for practical thruster operation.

### 6.1.1 CATHODE HEATER INTERLOCKS

To preclude overheating of the cathode inserts, the main cathode heater shall automatically turn off when the discharge current exceeds 5 amperes, and the neutralizer heater shall automatically turn off when the neutralizer keeper current exceeds 1 ampere.

### 6.1.2 HIGH VOLTAGE RECYCLE

The initiating conditions for high voltage are:

> Ion beam current exceeds 20A (adjustable between 10 and 20A) for 50 msec or accelerator (impingement) current exceeds 0.2A (adjustable between 0.05 and 0.2A) for 50 msec.

at t = 0

Turn off screen and accelerate voltages.

Decrease arc current to 15A (adjustable between 15 and 50A).

Increase neutralizer keeper current to 12A (adjustable between 5 and 15A).

at t = 200 msec (adjustable between 100 and 500 msec

Turn on screen and accelerate voltages.

at t = 300 msec

Increase arc current to previous setting.

Decrease neutralizer keeper current to previous setting.

The rise and decay times are:

| | Rise (msec) | Decay (msec) |
|---|---|---|
| Screen Voltage | < 50 | < 5 |
| Accel Voltage | < 50 | < 5 |
| Arc Current | 500 | 50 |
| Neut Keeper | < 5 | < 5 |

## 6.2 POWER SUPPLY SPECIFICATION

All power supplies to be continuously variable from 0 to maximum voltage, adjustable by front panel control. All supplies to be current limited, adjustable by front panel control.

### 6.2.1 POSITIVE HIGH VOLTAGE SUPPLY (Screen)

| | |
|---|---|
| Volts | 1200 |
| Amperes | 20 |
| Regulation | ±50V |
| Ripple (> 100 Hz) | ±5 percent |
| Output Impedance | > 1 μF |

### 6.2.2 NEGATIVE HIGH VOLTAGE SUPPLY (Accelerator)

| | |
|---|---|
| Volts | 600V |
| Amperes | 1A |
| Regulation | ±10V |
| Ripple (> 100 Hz) | ±5 percent |
| Output Impedance | > 0.1 μF |

### 6.2.3 MAIN DISCHARGE SUPPLY (Arc)

Operates at high voltage; requires isolated controls.

| | |
|---|---|
| Volts | 60V |
| Amperes | 100A |
| Regulation | ±1.5A |
| Ripple (> 100 Hz) | ±5 percent |
| Output Impedance | 0.5 mH |

### 6.2.4 CATHODE KEEPER SUPPLY

Operates at high voltage; requires isolated controls.

Start-up (boost) Mode

| | |
|---|---|
| Volts | 150V @ 0A |
| | 60V @ 0.1A |

Operate Mode

Operate in adjustable constant current mode.

| | |
|---|---|
| Volts | 30V |
| Amperes | 15A |
| Regulation | ±0.3A |
| Ripple (100 Hz) | ±5 percent |
| Output Impedance | No specification |

6.2.5 CATHODE TIP HEATER SUPPLY

Operate in constant current mode to protect refractory heater.

| | |
|---|---|
| Volts | 30V |
| Amperes | 30A |
| Regulation (power) | ±5 percent |
| Ripple (100 Hz) | ±10 percent |

6.2.6 NEUTRALIZER KEEPER SUPPLY

Start (boost) Mode)

| | |
|---|---|
| Volts | 150V @ 0A |
| | 60V @ 0.1A |

Operate Mode

Operate in adjustable constant current mode.

| | |
|---|---|
| Volts | 30V |
| Amperes | 10A |
| Regulation | ±0.15A |
| Ripple (100 Hz) | ±5 percent |
| Output Impedance | 2 mH |

### 6.2.7 NEUTRALIZER TIP HEATER SUPPLY

| | |
|---|---|
| Volts | 15V |
| Amperes | 20A |
| Regulation (power) | ±5 percent |
| Ripple ( 100 Hz) | ±10 percent |

### 6.2.8 MAIN FLOW CONTROL

Flow Measurement

Two (2) Hastings Raydist Flow Meters Model No. NALL-500 plumbed in parallel.

Flow Control

The minimum control system can use open loop, manual control with the flow control needle valves.

A more desirable system would provide closed loop control such as with Tylan mass flow controller Model FC-260 with a flow range of 10 to 500 sccm.

### 6.2.9 CATHODE FLOW CONTROL

Flow Measurement

Hastings Raydist Flow Meter Nodel No. NALL-100.

Flow Control

The minimum control system can use open loop, manual control with the flow control needle valves.

A more desirable system would provide closed loop control such as with Tylan mass flow controller Model FC-260 with a flow range of 10 to 500 sccm.

6.2.10 NEUTRALIZER FLOW CONTROL

Flow Measurement

Hastings Raydist Flow Meter Nodel No. NALL-10

Flow Control

The minimum control system can use open loop, manual control with the flow control needle valves.

A more desirable system would provide closed loop control such as with Tylan mass flow controller Model FC-260 with a flow range of 10 to 500 sccm.

## 6.3 INSTRUMENTATION

### 6.3.1 REQUIRED INSTRUMENTATION

The following parameters must be metered and available for control decisions:

| | |
|---|---|
| Positive High Voltage | V, I |
| Negative High Voltage | V, I |
| Main Discharge | V, I |
| Neutralizer Keeper | V, I |
| Main Flow | Standard cc/min |
| Cathode Flow | Standard cc/min |
| Neutralizer Flow | Standard cc/min |

### 6.3.2 RECOMMENDED INSTRUMENTATION

The following parameters are recommended for metering for efficiency measurements and diagnostics.

| | |
|---|---|
| Cathode Keeper | V, I |
| Cathode Tip Heater | V, I |
| Neutralizer Tip Heater | V, I |
| Cathode Tip Temperature | Pt, Pt-Rh TC |
| Neutralizer Tip Temperature | Pt, Pt-Rh TC |

# SECTION 7

# STUDY CONCLUSIONS

The program objective was to conduct the thermal, electrical, and mechanical analyses required to support the conceptual design of an electrostatic ion thruster meeting the requirements stated in table 7-1. The thruster design is based on both commercially available materials and on modular construction for ease of substitution of critical components. Scaleability is a prime consideration.

TABLE 7-1

THRUSTER GOALS

| Item | Argon | Xenon |
|---|---|---|
| Thrust | 0.5 newton | 0.5 newton |
| Specific Impulse, nominal | 6076 seconds | 3530 seconds |
| Specific Impulse Range | ±50 percent | ±50 percent |
| Efficiency | 0.68 | 0.74 |
| Lifetime | 15,000 hours | 15,000 hours |

The approach taken began with an evaluation of candidate plasma containment schemes based on the efficiency and scaleability goals. The selected concept was then refined through trade studies and design calculations defining configuration, size, and behavior. The results of these efforts were compiled in a conceptual design of a thruster meeting the design goals.

The resulting thruster is a 50 cm diameter electron bombardment gas discharge type that utilizes an alternating periodic magnet structure to contain the plasma. Significant design features include use of

either Alnico or samarium-cobalt permanent magnets to generate a boundary containment of the ionizing plasma, thus leaving the principal discharge volume very nearly field free. The discharge chamber length is a compromise between argon and xenon optimums. Also featured is an ion optics system adaptable to either two or three grid operation and taking advantage of inert gas properties to simplify the optics mounting and support over those traditionally used for the metallic propellants. A single cathode and single neutralizer complete the design.

In conducting the design analysis it was determined that the high power density of this thruster would require active cooling of the discharge chamber; radiation can reject less than half the discharge power at the upper temperature limit, the magnet degaussing temperature. Analyses also showed that grid spacing can be maintained at practical discharge chamber temperatures if the grids are performed to different radii of curvature in the cold (room temperature) state and allowed to expand into equal radii of curvature at operating temperature.

These two findings are based on mathematical modeling that needs to be confirmed with experimental data. Tests with 8 and 12 cm thrusters have proven the feasibility of both active cooling and preformed grids; however, the scale increase to 50 cm is too substantial a change to go unverified. A feasibility test should be conducted to gather thermal data both on discharge chamber cooling and ion optics response.

The trade studies indicated that a single cathode was preferable to multiple cathodes. The analysis indicated that adequate electrons would reach all areas of the discharge chamber and that a single cathode can deliver the required ionizing current. The operating temperature is more difficult to predict accurately. The critical

parameter of high current cathodes is lifetime so a demonstration of high current operation with cathode temperatures between 1000° and 1100°C should be undertaken.

In summary, a conceptual design has been developed for a high power, high thrust electrostatic ion thruster. Verification experiments have been identified to substantiate the analytical conclusions on which the design is based. Upon satisfactory completion of these experiments, the large inert gas thruster will be ready for detail design of a demonstration unit suitable for large space structure use.

BIBLIOGRAPHY


1. Brown, S. C., "Basic Data of Plasma Physics," MIT Press, Cambridge, Massachusetts, 1959

2. Dushman, S., "Scientific Foundations of Vacuum Technology," John Wiley and Sons, New York, 1962

3. Ferreira, C. M., and J. L. Delcrois, "Theory of the Hollow Cathode Arc," J. Appl. Phys, Vol. 49, No. 4, April 1978

4. Goebel, D. M., J. T. Crow, and A. T. Forrester, "Lanthanum Hexaboride Hollow Cathode for Dense Plasma Production," Rev. Sci. Instr. 49(4), April 1978

5. Goede, A. P. H., and T. S. Green, "Stability Limits to Ion Source Operation," Phys. Fluids, January 1978

6. Haines, "Plasma Containment in Cusp-Shaped Magnetic Fields," Nuclear Fusion Vol. 17, No. 4, 1977

7. Hershkowitz, Noah, K. N. Leung, and Thomas Romessert, "Plasma Leakage Through a Low-$\beta$ Line Cusp," Phys. Rev. Letters Vol. 35, No. 5, August 1975

8. Hirsch, Robert L., "Experimental Studies of a Deep, Negative, Electrostatic Potential Well in Spherical Geometry," Phys. Fluids Vol. II, No. 11, November 1968

9. Kitsunezaki, Akio, Mitsumori Tanimoto, and Tadashi Sekiguchi, "Cusp Confinement of High-Beta Plasmas Produced by a Laser Pulse from a Freely-Falling Deuterium Ice Pellet," Phys. Fluids Vol. 17, No. 10, October 1974

10. Kozlov., N. P., and Yu S. Protasov, "Effect of Electric Field on Non-Ideal Plasma Conductivity, " Phys. Letters Vol. 51A, No. 8 May 1975

11. Krishnan, M., R. G. Jahn, W. F. Jaskowsky, and K. E. Clark, Physical Processes in Hollow Cathodes," AIAA J. Vol. 15, No. 9, September 1977

12. Leung, K. N., R. D. Collier, G. R. Taylor, and R. E. Kribel, "Increasing the Ion Beam Current from a Multidipole Source," Appl. Phys. Letters, Col. 31, No. 3, August 1977

13. Leung, K. N., R. E. Kribel, D. G. Fitzsimons, and G. R. Taylor, "Plasma Leakage Velocity Through a Low $\beta$ Line Cusp," Phys. Letters Vol. 60A, No. 3, March 1977

14. Leung, K. N., and R. D. Collier, et al, "Characteristics of a Multidipole Ion Source," Rev. Sci. Instr. Vol. 49, No. 3, 3 March 1978

BIBLIOGRAPHY (contd)


15. Leung, Samec, and Lamm, "Optimization of Permanent Magnet Confinement," Phys. Letters Vol. 51A, No. 8, May 1975

16. Limpaecher, Rudolph, and K. R. McKenzie, "Magnetic Multipole Containment of Large Uniform Collisionless Quiescent Plasmas," Rev. Sci. Instr., Col. 44, No. 6, June 1973

17. Martin, R. J., and J. E. Rowe, "Experimental Investigation of the Low-Voltage Arc in Nobel Gases," J. Appl. Phys. Vol. 39, No. 9, pp. 4289-4298, August 1968

18. Masek, "Plasma Properties and Performance of Mercury Ion Thrusters," AIAA 7th Elec. Propulsion Conf. Paper 69-256

19. Moore, R. David, "Magneto-Electrostatically Contained Plasma Ion Thruster," AIAA Paper No. 69-260, AIAA 7th Elec. Propulsion Conf., Williamsburg, Virginia, March 1969

20. Nakamura, Y., B. H. Quon, and A. Y. Wong, "Ion Confinement by Electrostatic Potential Well in Magnetic Multipole Device," Phys. Letters Vol. 53A, No. 1, May 1975

21. O'Donnell, W. J., and B. F. Langer, "Design of Perforated Plates," J. Eng. Industry, August 1962

22. Poeschel, R. L. et al, "30 cm Mercury Ion Thruster Technology," AIAA/DGLR 14th Internatl. Elec. Propulsion Conf., October 30-November 1, 1979, Princeton, New Jersey

23. Poeschel, R. L., and J. R. Beattie, "Primary Electric Propulsion Technology Study," Section 3, Robinson, Cathode Lifetime, NASA CR-159688, November 1979

24. Ramsey, W. D., "12 cm Argon/Xenon Ion Source," AIAA 13th Elec. Propulsion Conf. Paper No. 78-681, San Diego, April 1978

25. Ramsey, W. D., "Inert Gas Ion Source," Section 2.13 - Preliminary Cathode Tests, NASA CR-159423, July 1978

26. Ramsey, W. D., and E. L. James, "A Prototype North-South Station-keeping Thruster," AIAA/SAE 10th Propulsion Conf., San Diego, October 1974

27. Schott, L., "Plasma Enclosed in a Magnetic Field Produced by Flexible Surface Magnets," Rev. Sci. Instr. 49(4), April 1978

28. Siegfried, D., and P. J. Wilbur, "Studies on an Experimental Quartz Tube Hollow Cathode," AIAA Paper No. 79-2056, October 1979

BIBLIOGRAPHY (contd)


29. Siegfried, D., and P. J. Wilbur, "An Investigation of Mercury Hollow Cathode Phenomena," AIAA Paper No. 79-705, April 1978

30. Speiser, R. C. et al, "Cesium Electron Bombardment Thruster Research," Contract NAS7-587 Final Report, October 1968

31. Stirling, W. L., C. C. Tsai, and P. M. Ryan, "15 cm DuoPigatron Ion Source," Rev. Sci. Instr. Vol. 48, No. 5, May 1977

32. Stirling, W. L., P. M. Ryan, C. C. Tsai, and K. N. Leung, "Magnetic Multipole Line Cusp Plasma Generator for Neutral Beam Injectors," Rev. Sci. Instr. Vol. 50, No. 1, January 1979

33. Spitzer, L., Physics of Fully Ionized Gases, 2nd Ed., John Wiley and Sons, New York, 1962

34. Touloukian, Y. S., Editor, "Thermophysical Properties of Matter," IFI Plenum, New York, 1970

35. Tsai, C. C., W. L. Stirling, and P. M. Ryan, "Plasma Studies on a DuoPigatron Ion Source," Rev. Sci. Instr., Vol. 48, No. 6, June 1977

36. Zafran, S., "Ion Engine Auxiliary Propulsion Applications and Integration Study," NASA CR-135312, July 1977

37. Zavesky, R., "LeRC 30 cm Thruster Grid System Thermal Measurements," Private Communication, 1979